Summer 2016

Study jitter amplification of a passive channel and investigation of S_{21} magnitude extraction methodologies using a pattern generator and oscilloscope

Xinyun Guo

STUDY JITTER AMPLIFICATION OF A PASSIVE CHANNEL AND

INVESTIGATION OF S_{21} MAGNITUDE EXTRACTION METHODOLOGIES USING

A PATTERN GENERATOR AND OSCILLOSCOPE

by

XINYUN GUO

A THESIS

Presented to the Faculty of the Graduate School of the

MISSOURI UNIVERSITY OF SCIENCE AND TECHNOLOGY

In Partial Fulfillment of the Requirements for the Degree

MASTER OF SCIENCE

in

ELECTRICAL ENGINEERING

2016

Approved by
Dr. Jun Fan, Advisor
Dr. James L. Drewniak
Dr. David Pommerenke

ABSTRACT

Recently the clock channel jitter amplification has been observed, modeled and measured in several publications [1][2][3][5]. Currently in many high-speed I/O systems, to avoid the cost and the complex clock recovery circuit design, people use traces forwarding clock signal from transmitting IC to receiving IC. When these clock traces are long enough, the amount of attenuation will induce not only inter-symbol-interference (ISI) but also modulate with the input jitter. Eventually it will lead some type of jitter been amplified after the channel. Similarly, the high speed communication channel (data channel) will also face this issue. Since there are no studies on the jitter amplification in a data channel, it will be studied in this section. This part of study includes verifying and confirming this phenomenon in a clock channel. A more generalized periodic jitter amplification equation has been developed. Then, it compared different types of jitter changing trend after lossy channels using different data patterns as sources.

The second part of the thesis is to investigate S_{21} magnitude extraction methods using an oscilloscope and pattern generator. S-parameter measurements of a digital link path are measured with VNAs or high-end TDRs. For multi-port in-situ measurements, these become inconvenient and time consuming. However, it can be handled more conveniently in the time domain (TD) by using a pattern generator and a multi-channel sampling oscilloscope, which are used for eye-diagram measurements. This part of work outlines and compares three methods to extract S21 magnitude from the time domain measurements using a pattern generator and a sampling oscilloscope for any channel. The setup differs in terms of the input waveform and the processing. The comparison provides insight into the advantages and limitations of each method.

ACKNOWLEDGMENTS

First of all I would like to use this chance and thank my advisor Dr. Jun Fan for his patiently guidance during my master study. Dr. Fan gives me a lot of useful guidance and advice not only for my research and study but also for my daily life and future work. I would express my sincerely thanks to him.

I would like to specially thank Dr. James Drewniak for encouraging me and supporting me when I have chance to study in the industry. Dr. Drewniak helps me on the career planning and building strong professional skills. I would sincerely thanks for his supporting during my study in the EMC lab.

I would also like to thanks all the students and faculties that I worked with in the EMC lab. Their supporting and encouragement make me be able to finish my master degree today.

Finally, I would like to thank my beautiful family. My parents and my sister Xinyao, they give their endless love to me as always, it is their love and support make stronger and stronger. My husband Tianqi Li, he is a good mentor, a lovely friend. It is him who helps and accompanies me through all the difficulties during my graduate study. I would like to thank for his love, trust and support during my graduate study.

TABLE OF CONTENTS

LIST OF ILLUSTRATIONS

1. STUDY JITTER AMPLIFICATION OF A PASSIVE CHANNEL

1.1. IINTRODUCTION

Jitter amplification is defined as the ratio of the output jitter to the input jitter, and it happens when the ratio is larger than one [1]. In the past several years, there are some publications [1][2][3][5] discuss the jitter amplification in clock channels. Three types of jitter components have been found can be amplified: duty-cycle-distortion (DCD), sinusoidal jitter (SJ) and random jitter (RJ) [3]. Jitter is amplified even when the channel is linear passive and noiseless [3]. The amplification is due to the channel loss. Jitter lower sideband (LSB) has less attenuation than the attenuation at the signal carrier and it leads to jitter increasing after the channel. The benefit of studying clock channel is because the data dependent jitters (DDJ) like intersymbol interference (ISI) is zero due to the natural characteristic of 1010 clock pattern. To study the amplification of each type of jitter, one should obtain only this type of jitter at both input and output of channel. When using a non-clock signal as source, the DDJ should be removed at the output from the total jitter (TJ).

1.2. JITTER TYPES

Jitter can be classified using two criteria: first is whether it is bounded, second is whether it is correlated. Fig.1.1 is shown the different jitter components in the total jitter. Based on the first criteria total jitter can be break down into deterministic jitter (DJ) and random jitter (RJ). Further deterministic jitter can break into bounded correlated jitter - data dependent jitter (DDJ), bound uncorrelated jitter (BUJ) and periodic jitter (PJ). DDJ is composed of duty cycle distortion (DCD) and intersymbol interference (ISI).
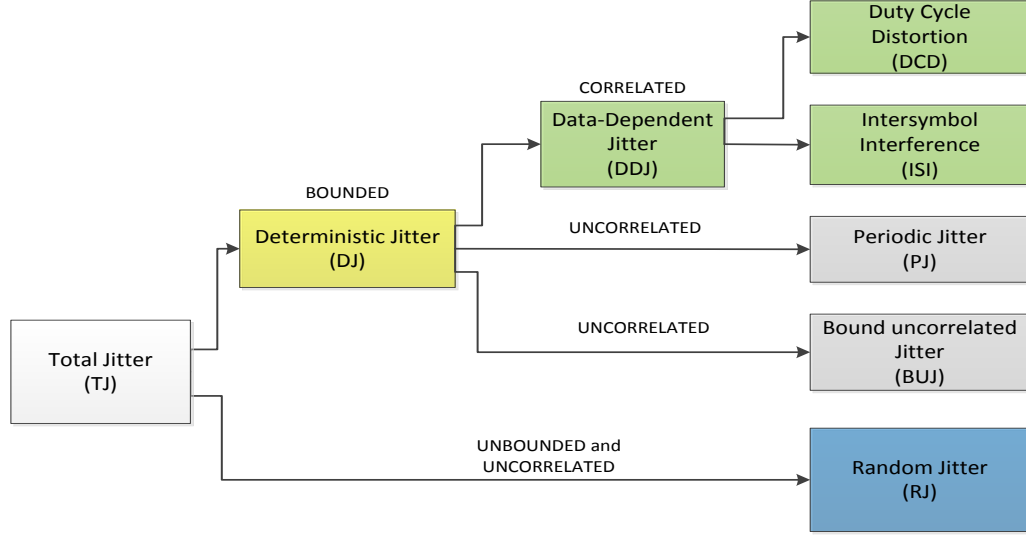
Figure 1.1. Jitter Components.

Fig. 1.1 is showing the complete system of jitter components. When studying the jitter amplification using non-clock source, one important step is to decompose PJ or RJ and DDJ. Therefore, knowing each type of jitter component in total jitter is very helpful for later jitter seperation. Clock waveform is not affected by ISI. In our study, we focus on RJ and PJ amplification analysis.

1.2.1. Periodic Jitter. Periodic jitter is the periodic variation in the phase of the data stream. This type of jitter is uncorrelated to the stream and is bounded. The time interval error of this type of jitter is a periodic signal (sine wave). It is usually caused by some external coupling into the circuit, power supply noise, PLL comparator frequency feed-through. An approximation of PJ probability distribution can be a dual- Dirac delta function as shown in Fig. 1.2. PJ distribution function (PDF) [7] can be defined as

$$f_{PJ}(\Delta t) = \frac{1}{\pi\sqrt{1-(\Delta t / A)^2}}, -A \leq \Delta t \leq A$$
$$0, otherwise$$

(1.1)

where A is the peak to peak magnitude of PJ. So the PJ peak to peak amplitude can be also read from its jitter distribution.
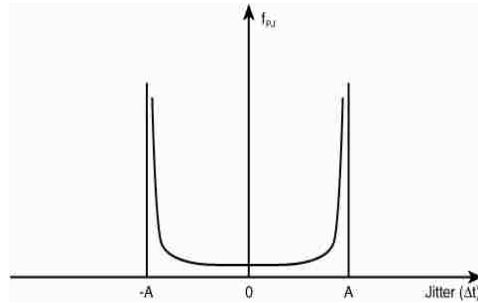
Figure 1.2. Periodic jitter probability distribution.

1.2.2. Random Jitter. Random jitter is the random variation in the phase of the data stream. This type of jitter is uncorrelated to the stream and is unbounded. The time interval error of this type of jitter is Gaussian distribution as shown in Fig. 1.3. It is usually caused by thermal noise, shot noise, flicker noise etc. RJ PDF can be defined as

$$f_{RJ}(\Delta t) = \frac{1}{\sqrt{2\pi}\delta} e^{-\frac{(\Delta t)}{2\delta^2}}$$

(1.2)

where δ is standard deviation.
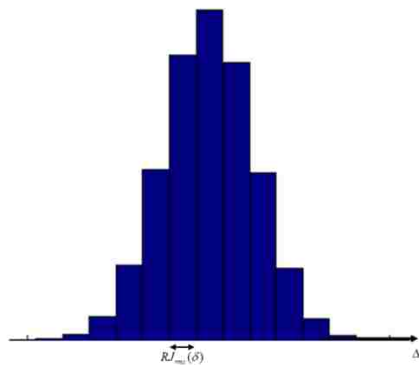
Figure 1.3. Random jitter probability distribution.

A reasonable approximation of the peak-to-peak value of RJ depends on the BER and is related to the RMS value of RJ by the following equation:

$$RJ_{PP} = \alpha * RJ_{rms}$$ (1.3)

where the value of α (scaling factor) is calculated from the BER. The ratio of RMS jitter value will be used to monitor the jitter amplification of the lossy channels.

1.2.3. Intersymbol Interference. Intersymbol interference is the jitter due to the bandwidth limitations in the channel used for transmitting the data stream. This type of jitter is correlated and bounded. This type of jitter has no specific mathematical model. It is best modeled by a filter and is specified by its bandwidth. It is usually caused by the channel whose impulse response is longer than a data bit. In our study this type of jitter is taking large part porting in the total jitter distribution due to we have lossy channel and it should be filtered out after jitter decomposition.

1.3. TIME INTERVAL ERROR

Time interval error (TIE) is the difference between the observed edge time and the expected edge time for each edge present in a data stream. The time-interval error measures the zero crossing transitions of the measured waveform against its ideal counterpart. The ideal counterpart is well represented by a jitter free clock. It can be explained using a simple equation as

Measured arrival time of an edge − Expected arrival time of the edge = TIE for the edge   (1.4)

It describes how early or late an edge arrives compared to its expected arrival time. Fig. 1.4 (a) shows the edges time difference between the output waveform verses the jitter free clock at the zero crossing point, and (b) is showing the calculated raw TIE and after interpolation. There are no transition occur at some positions in the data

waveform. The code is using a linear interpolation and adding TIE points on those transition edges.

(a)

(b)
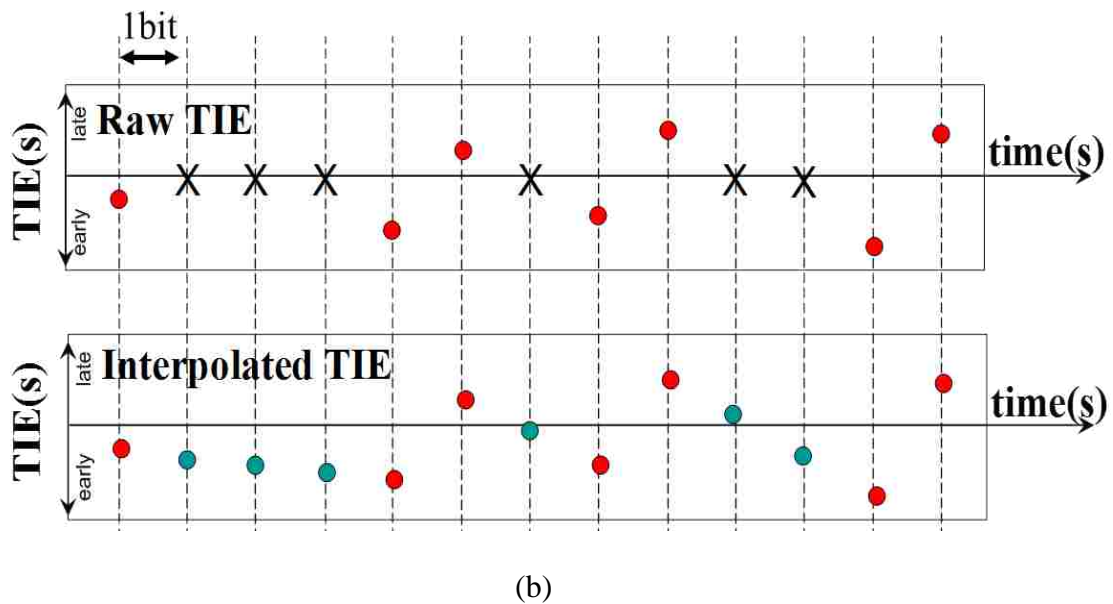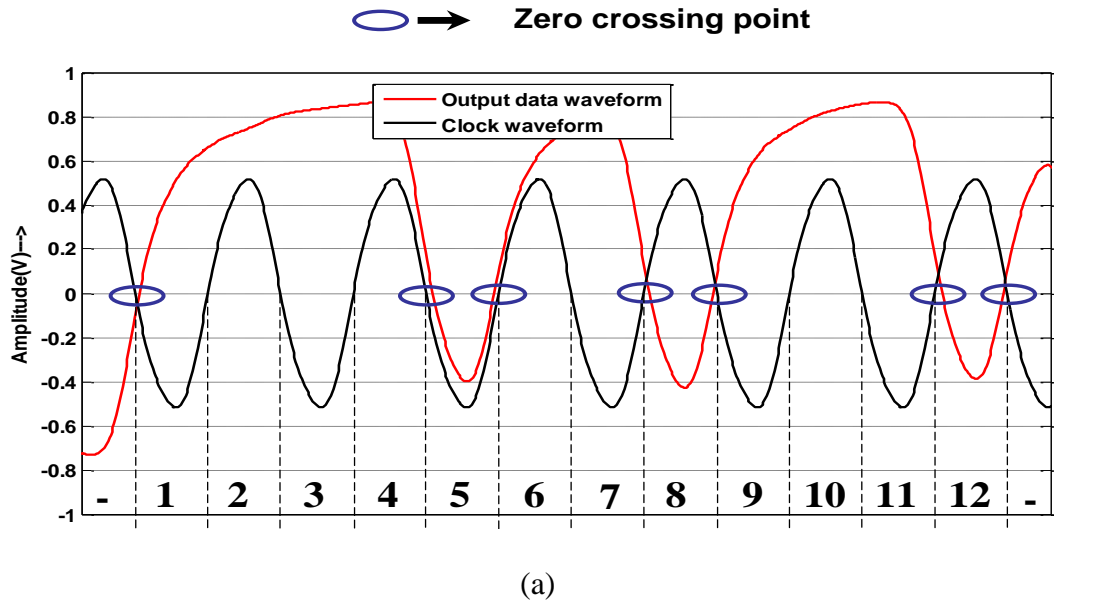
Figure 1.4. TIE extraction. (a) Real output waveform vs reference clock waveform (b) its raw TIE waveform vs its interpolated TIE waveform.

If a time-to-frequency domain operation or transfer is made to TIE time domain waveform, the jitter frequency representation is obtained. Fig. 1.5 is showing a jitter spectrum containing all jitter components.
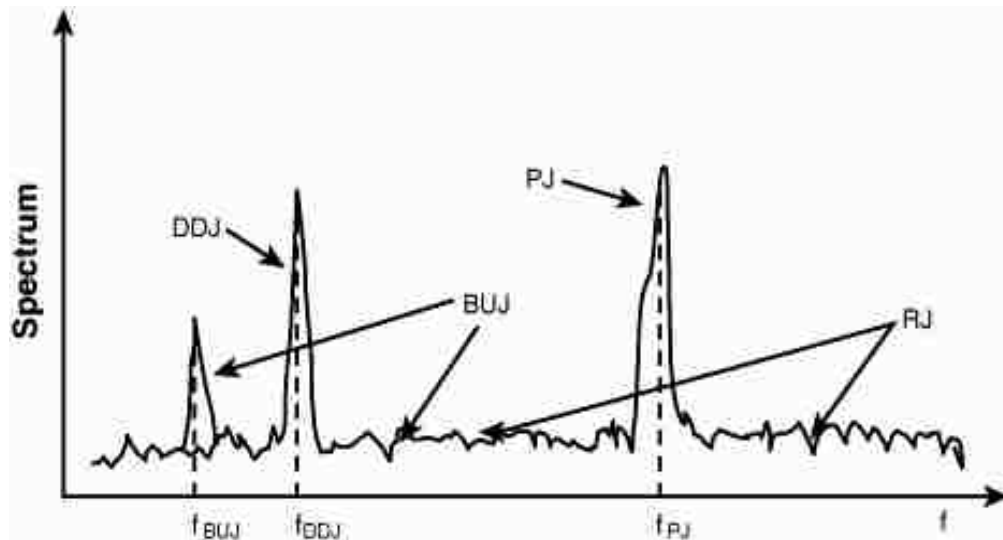
Figure 1.5. Jitter spectrum with all the components present.

Each jitter components has certain and unique characteristics [7]. Periodic jitter shows up as spikes or spectral lines in the according frequency in the frequency domain. DDJ is associated with repeating pattern, DDJ also shows up spikes or spectral lines. Their frequency is integer multiples of the pattern frequency $f_{pattern}$, where

$f_{pattern} = 1/(N_{pattern} * UI)$ and $N_{pattern}$ is the length of the pattern in terms of UI. BUJ and RJ show up as broadband bound background noise.

In our study, to simply the problem, we inject RJ and PJ separately in the source. Therefore we only need to separate the PJ or RJ with the DDJ. BUJ is majorly caused by crosstalk, we don't have differential channel in the study so that we'll not have BUJ.

1.3.1.   TIE Calculation. TIE is been used to monitor jitter's changing trend in

the study. To calculate a TIE waveform, Keysight ADS circuit simulation has been used

for generating the testing waveforms. Fig 1.6 shows the example circuits used for

generating two waveforms. The output waveform is generating using Fig. 1.6 (a). The

output waveform must be compared with an ideal counterpart, which is a jitter free

waveform that is generated using Fig. 1.6 (b).

(a)

(b)
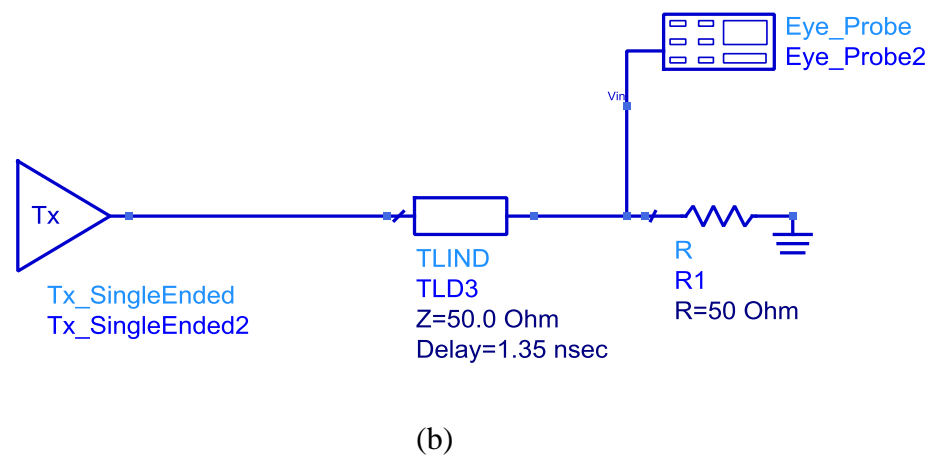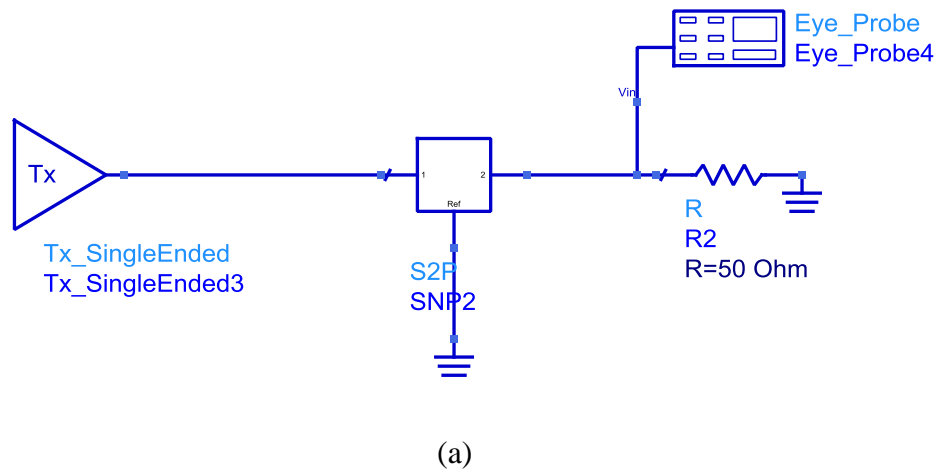
Figure 1.6. ADS simulation circuits example. (a) Tx + RJ/PJ + lossy transmission line (b)
Tx + RJ/PJ + ideal transmission line (with same delay).

Fig. 1.7 shows the general approach for obtaining the TIE waveform. By detecting the time position difference at the zero crossing level, the TIE can be detected. Because the frequency domain waveform needs to be used for some observation later, so the Raw TIE has been interpolated to improve the upper bandwidth.
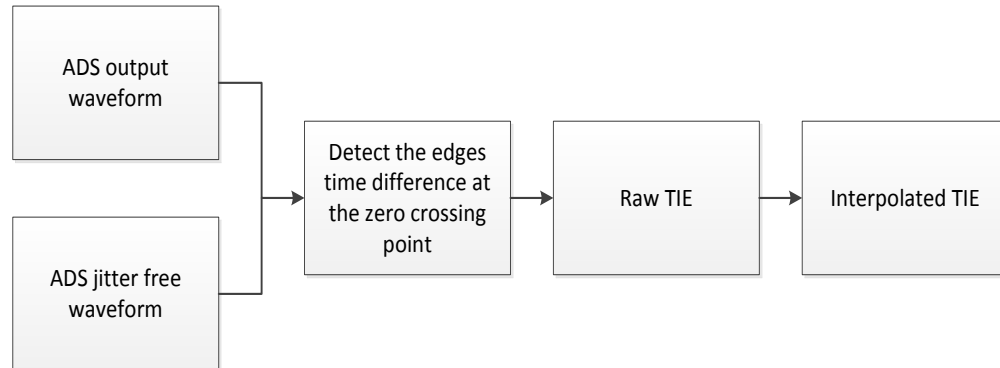
Figure 1.7. TIE calculation general procedures.

1.3.2.   PJ TIE. Periodic jitter is added using Keysight ADS channel simulation "Tx_SingleEnded" block. The generated periodic jitter's TIE waveform is a periodic signal (sinewave), so it can also be called as sinusoidal jitter. Figure 1.8 (a) is a 1 GHz periodic jitter with a 5ps peak-to-peak magnitude. The according TIE spectrum is showing Figure 1.8 (b).Because the source waveform is using a clock waveform, each "X" symbol in (a) is representing a time difference at the each transition point compare to reference clock (jitter free clock). The TIE spectrum shows the 1GHz PJ frequency and 5ps magnitude which is same as our simulation settings.

Because we are using clock signal as input so we are not expecting to see the ISI or any other DDJ components in both time and frequency domain TIE.

(a)   (b)
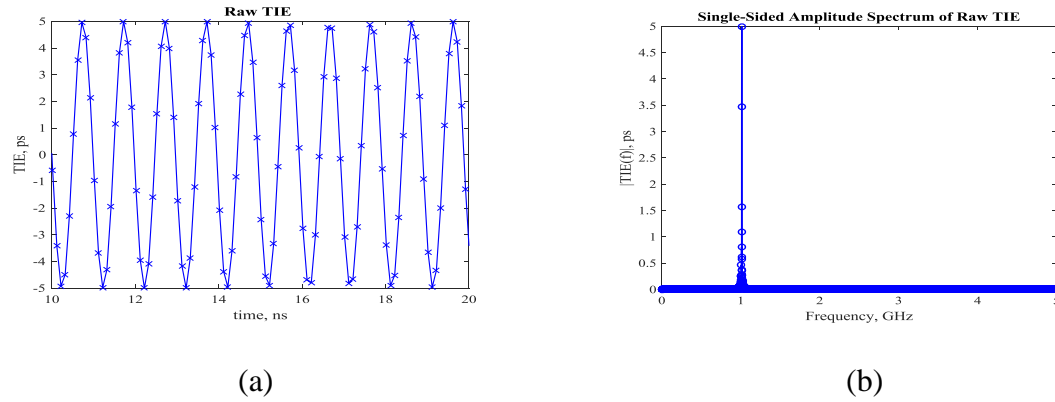
Figure 1.8. 1GHz PJ. (a) time domain TIE (b) frequency domain TIE.

The spectrum is created using Matlab Fast Fourier Transform (FFT), and it is using the TIE time domain waveform. TIE time domain and spectrum domain waveforms have been used to monitor the PJ changing trend in the amplification study.

1.3.3. RJ TIE. Random jitter is added using Keysight ADS channel simulation "Tx_SingleEnded" block. RJ's standard deviation (σ) is been setup as 1% of UI (unit interval), which is 1ps RMS value of RJ. The generated random jitter's TIE waveform is a band limited white noise. Figure 1.9 (a) is a RJ with 1ps rms value in time domain, (b) is its according spectrum domain waveform.

(a)   (b)
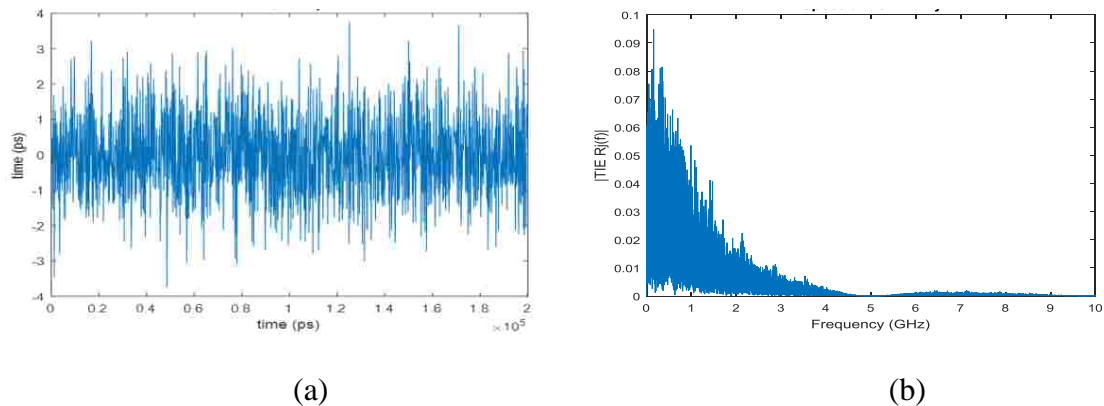
Figure 1.9. A RJ rms value is 5ps. (a) Time domain TIE (b) Frequency domain TIE.

1.3.4. Jitter Separation Procedure. TIE simulation has been used to study and monitor jitter's changing trend and verifying the equation predicted amplification result. The process is done by Matlab. The major steps are shown in the following flow chart in Fig1.10. Especially, for PRBS case, the amount of DDJ is dominant. However, DDJ is not the jitter component that we want to study. So it has to be removed to give us the value of only RJ or PJ. There are many ways to remove DDJ, a common method has been chosen for current application [4].
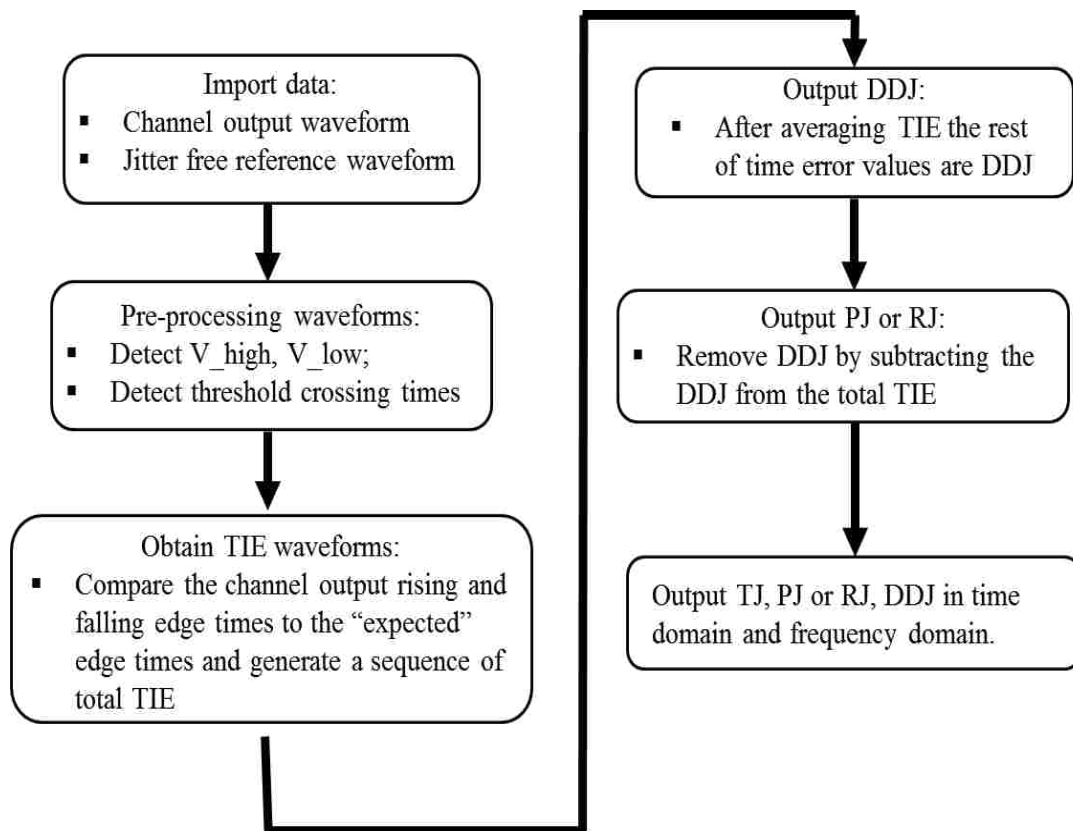
Figure 1.10. Jitter separation procedure.

There is a set of output waveform in both time and frequency domain has been used as an example in Fig.1.11. The input signal is a 7Gbps PRBS3 with a peak to peak

value about 4.5ps PJ at 0.512GHz. Before jitter separation the total jitter peak to peak value is quite large. The spectrum shows that there is some other spectrum component except 0.512 GHz PJ component. These are the DDJ which happen when channel is too lossy. After removing DDJ, the PJ TIE shows that PJ amplitude a little bit larger than 4.5ps. PJ's spectrum shows that the majority of DDJ has been removed.
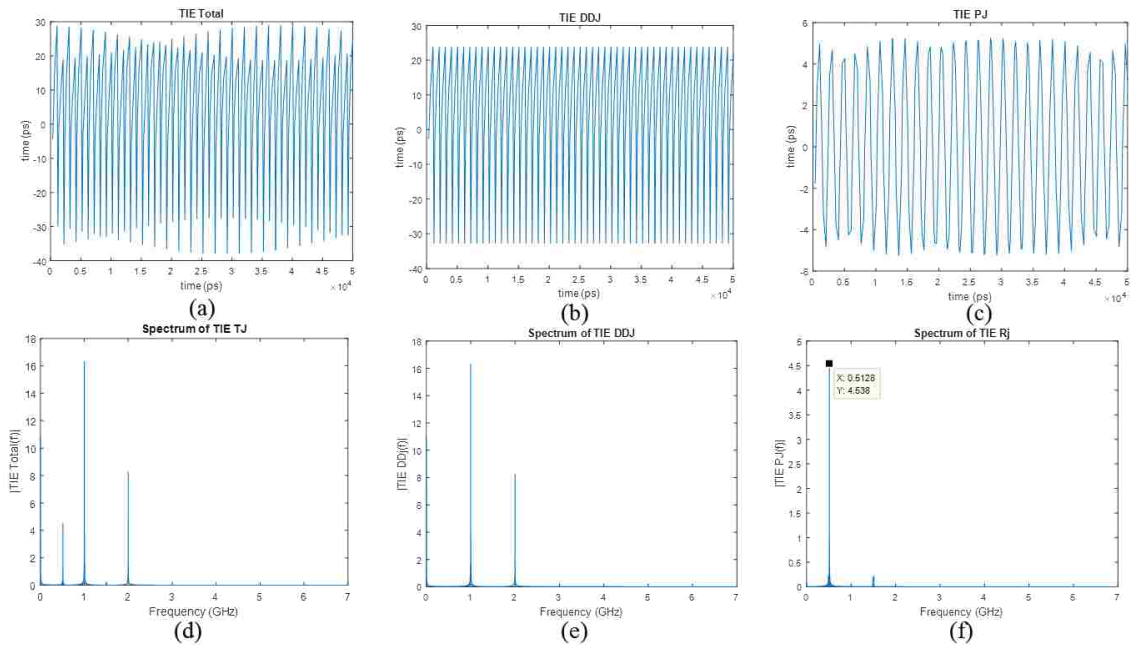
Figure 1.11. TIE in time domain (TD) and frequency domain (FD) (a) Total TIE in TD (b) TIE DDJ in TD (c) TIE PJ in TD (d) Total DDJ in FD (e) TIE DDJ in TD (f) TIE PJ in FD.

1.4. PERIODIC JITTER AMPLIFICATION

Due to the frequency modulation (PM), the clock spectrum has been shifted and split into the lower sideband and upper side band [3]. After lossy channel the higher order harmonics are heavily attenuated. PJ's amplification factor can be predicted using the jitter transfer function of these two components. It shown that amplification factor is increasing exponentially with the clock data rate. In addition, PJ in a clock channel is

amplified by lossy channels at any frequency below Nyquist frequency. This has been confirmed using numerical simulation approach. Also a case when jitter frequency larger than Nyquist frequency has also been studied. The amplification factor shows a periodic pattern as the jitter frequency increasing, which due to the phase modulation mechanism. A mathematical model has been developed to describe the jitter's changing trend. The equation has been verified by simulation results. In the last part of this section is to find out the PJ's changing rend in a PRBS Channel. The simulation results show s that the PJ amplification factor is shown similar periodic pattern as the clock when PJ frequency is increasing. When the jitter frequency is smaller than all the PRBS harmonic frequencies, an equation has been used to predict PJ's amplification.

1.4.1. Frequency Modulation. Frequency modulation is common term has been used in the telecommunications and signal processing. It is the encoding of the information in a carrier wave by varying the instantaneous frequency of the wave. It can be used to describe the clock and periodic jitter transformation.

In the clock channel with a PJ case, due to the clock higher order harmonic has been heavily attenuated by the lossy channel. The clock can be approximated into a sinusoidal wave with a single tune jitter. The mathematical forms are:

$$v_{in}(t) = A\cos[\omega_0 t + \theta_0 + \phi(t)] \tag{1.4}$$

A sinusoidal jitter with a frequency ω expression is:

$$\phi(t) = \int_{-\infty}^{+\infty} \phi(\omega) e^{j\omega t} \, d\omega \tag{1.5}$$

when jitter $\phi(t)$ is small, in the frequency modulation, only the Bessel coefficients $J_0(\beta)$ and $J_1(\beta)$ have significant values. Therefore signal is effectively

composed of a carrier and a single pair of side frequencies at $f_{carrier} \pm f_{modulation}$. The jitter

expression can be written as:

$$\phi(t) = \phi(\omega)\,e^{j\omega t} + \phi(\omega)^* \, e^{-j\omega t} \tag{1.6}$$

Then substitute Eq.1.6 into Eq.1.4,

$$
\begin{aligned}
v_{in}(t) &= \frac{A}{2}[e^{j(\omega_0 t+\theta_0)} + j\phi(t)\,e^{j(\omega_0 t+\theta_0)} + e^{-j(\omega_0 t+\theta_0)} - j\phi(t)\,e^{-j(\omega_0 t+\theta_0)}] \\
&= \frac{A}{2}\{e^{j(\omega_0 t+\theta_0)} + j[\phi(\omega)\,e^{j\omega t} + \phi(\omega)^* \, e^{-j\omega t}]e^{j(\omega_0 t+\theta_0)} \\
&\quad + e^{-j(\omega_0 t+\theta_0)} - j[\phi(\omega)\,e^{j\omega t} + \phi(\omega)^* \, e^{-j\omega t}]e^{-j(\omega_0 t+\theta_0)}\} \\
&= \frac{A}{2}[e^{j(\omega_0 t+\theta_0)} + j\phi(\omega)\,e^{j\omega t+j(\omega_0 t+\theta_0)} + j\phi(\omega)^* \, e^{-j\omega t+j(\omega_0 t+\theta_0)} \\
&\quad + e^{-j(\omega_0 t+\theta_0)} - j\phi(\omega)\,e^{j\omega t-j(\omega_0 t+\theta_0)} - j\phi(\omega)^* \, e^{-j\omega t-j(\omega_0 t+\theta_0)}]
\end{aligned}
\tag{1.7}
$$

Eq.1.7 shows that the frequency modulation spectrum is shifted by the carrier and

split into the lower side band $\omega_0 - \omega$, the upper sideband at $\omega_0 + \omega$, and their complex

conjugates. The output voltage after channel can be written as:

$$
\begin{aligned}
v_{out}(t) &= \frac{A}{2}\mathrm{H}(\omega_0)e^{j(\omega_0 t+\theta_0)}[e^{-\mathrm{Im}\{\psi_+(t)\}}e^{j\mathrm{Re}\{\psi_+(t)\}}] + \{\frac{A}{2}\mathrm{H}(\omega_0)e^{j(\omega_0 t+\theta_0)}[e^{-\mathrm{Im}\{\psi_+(t)\}}e^{j\mathrm{Re}\{\psi_+(t)\}}]\}^* \\
&= Ae^{-\mathrm{Im}\{\psi_+(t)\}}\mathrm{H}(\omega_0)\{\frac{e^{j\angle \mathrm{H}(\omega_0)}e^{j(\omega_0 t+\theta_0)}\,e^{j\mathrm{Re}\{\psi_+(t)\}}}{2} + \frac{[e^{j\angle \mathrm{H}(\omega_0)}e^{j(\omega_0 t+\theta_0)}\,e^{j\mathrm{Re}\{\psi_+(t)\}}]^*}{2}\} \\
&= Ae^{-\mathrm{Im}\{\psi_+(t)\}}\mathrm{H}(\omega_0)\mathrm{Re}\{e^{j\angle \mathrm{H}(\omega_0)}e^{j(\omega_0 t+\theta_0)}\,e^{j\mathrm{Re}\{\psi_+(t)\}}\} \\
&= Ae^{-\mathrm{Im}\{\psi_+(t)\}}\mathrm{H}(\omega_0)\cos(\angle \mathrm{H}(\omega_0) + \omega_0 t + \theta_0 + \mathrm{Re}\{\psi_+(t)\})
\end{aligned}
\tag{1.8}
$$

Then defined $\psi_+(t)$ and $\psi_-(t)$:

$$
\begin{cases}
\psi_+(t) = \dfrac{\mathrm{H}(\omega_0+\omega)\phi(\omega)\,e^{j\omega t}}{\mathrm{H}(\omega_0)} + \dfrac{\mathrm{H}(\omega_0-\omega)\phi(\omega)^* \, e^{-j\omega t}}{\mathrm{H}(\omega_0)} \\[3mm]
\psi_-(t) = \dfrac{\mathrm{H}(-\omega_0+\omega)\phi(\omega)\,e^{j\omega t}}{\mathrm{H}(-\omega_0)} + \dfrac{\mathrm{H}(-\omega_0-\omega)\phi(\omega)^* \, e^{-j\omega t}}{\mathrm{H}(-\omega_0)}
\end{cases}
\tag{1.9}
$$

where $\text{Re}\{\psi_+(t)\}$ and $\text{Im}\{\psi_+(t)\}$ are real and imaginary part of $\psi_+(t)$, respectively. While the phase term $\angle H(\omega_0)$ represents the delay of the channel, the phase modulation in the output signal is given by $\text{Re}\{\psi_+(t)\}\ \text{Re}\{\psi_+(t)\}$.

$$
\begin{aligned}
\phi_{out}(t) &= \text{Re}\{\psi_+(t)\} \\
&= \frac{1}{2}[\psi_+(t) + \psi_+(t)^*] \\
&= \frac{1}{2}[\frac{H(\omega_0+\omega)\phi(\omega)e^{j\omega t}}{H(\omega_0)} + \frac{H(\omega_0-\omega)\phi(\omega)^* e^{-j\omega t}}{H(\omega_0)} + \frac{H(\omega_0+\omega)^* \phi^*(\omega)e^{-j\omega t}}{H(\omega_0)^*} + \frac{H(\omega_0-\omega)^* \phi(\omega)e^{j\omega t}}{H(\omega_0)^*}] \\
&= \frac{1}{2}\{[\frac{H(\omega_0+\omega)}{H(\omega_0)} + \frac{H(\omega_0-\omega)^*}{H(\omega_0)^*}]\phi(\omega)e^{j\omega t} + [\frac{H(\omega_0-\omega)}{H(\omega_0)} + \frac{H(\omega_0+\omega)^*}{H(\omega_0)^*}]\phi(\omega)^* e^{-j\omega t}\} \\
&= \frac{1}{2}\{[\frac{H(\omega_0+\omega)}{H(\omega_0)} + \frac{H(\omega_0-\omega)^*}{H(\omega_0)^*}]\phi(\omega)e^{j\omega t} + c.c.\} \\
&= \frac{1}{2}\text{Re}\{[\frac{H(\omega_0+\omega)}{H(\omega_0)} + \frac{H(\omega_0-\omega)^*}{H(\omega_0)^*}]\phi(\omega)e^{j\omega t}\} \\
&= \frac{1}{2}\left|\frac{H(\omega_0+\omega)}{H(\omega_0)} + \frac{H(\omega_0-\omega)^*}{H(\omega_0)^*}\right||\phi(\omega)|\cos\{\angle[\frac{H(\omega_0+\omega)}{H(\omega_0)} + \frac{H(\omega_0-\omega)^*}{H(\omega_0)^*}] + \angle[\phi(\omega)] + \omega t\}
\end{aligned}
$$
(1.10)

The injected PJ is:

$$
\phi(t) = \phi(\omega)e^{j\omega t} + \phi(\omega)^* e^{-j\omega t} = |\phi(\omega)|\cos[\angle\phi(\omega) + \omega t]
$$
(1.11)

Therefore the transfer function can be written as:

$$
F_{SJ}(\omega) = \frac{1}{2}\left|\frac{H(\omega_0+\omega)}{H(\omega_0)} + \frac{H(\omega_0-\omega)^*}{H(\omega_0)^*}\right|
$$
(1.12)

The PJ amplification is the PJ transfer function of the two modulation terms. When the jitter frequency is smaller than Nyquist frequency, the equation is valid. However, when the jitter frequency is larger than the Nyquist frequency, the equation cannot continue be used to predict PJ's jitter amplification. Because when jitter frequency is larger than the Nyquist frequency of the clock, the jitter will be under sampled and then shifted to another frequency. Fig.1.12 is shown a normal sample example using TIE.
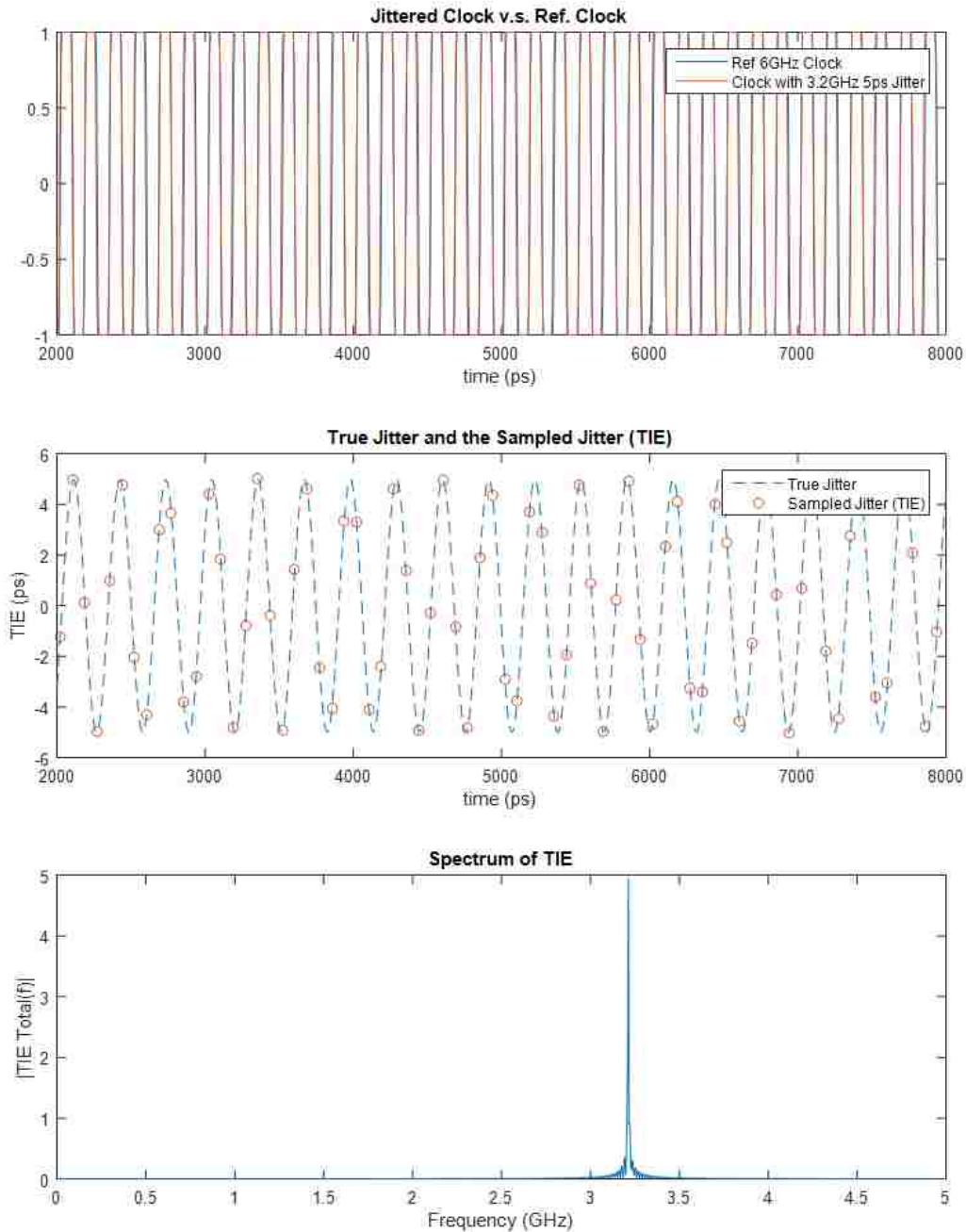
Figure 1.12. Normal sampled case.

The normal sampled case is showing the Nyquist frequency is 6GHz clock with a

3.213GHz periodic jitter. The time domain TIE is comparing the sampled jitter at the

edge of the clock to the true jitter (the injected jitter). Both time and frequency domain

TIE shows that in this case PJ has been correct sampled. Fig.1.13 is shown a under sampled case.
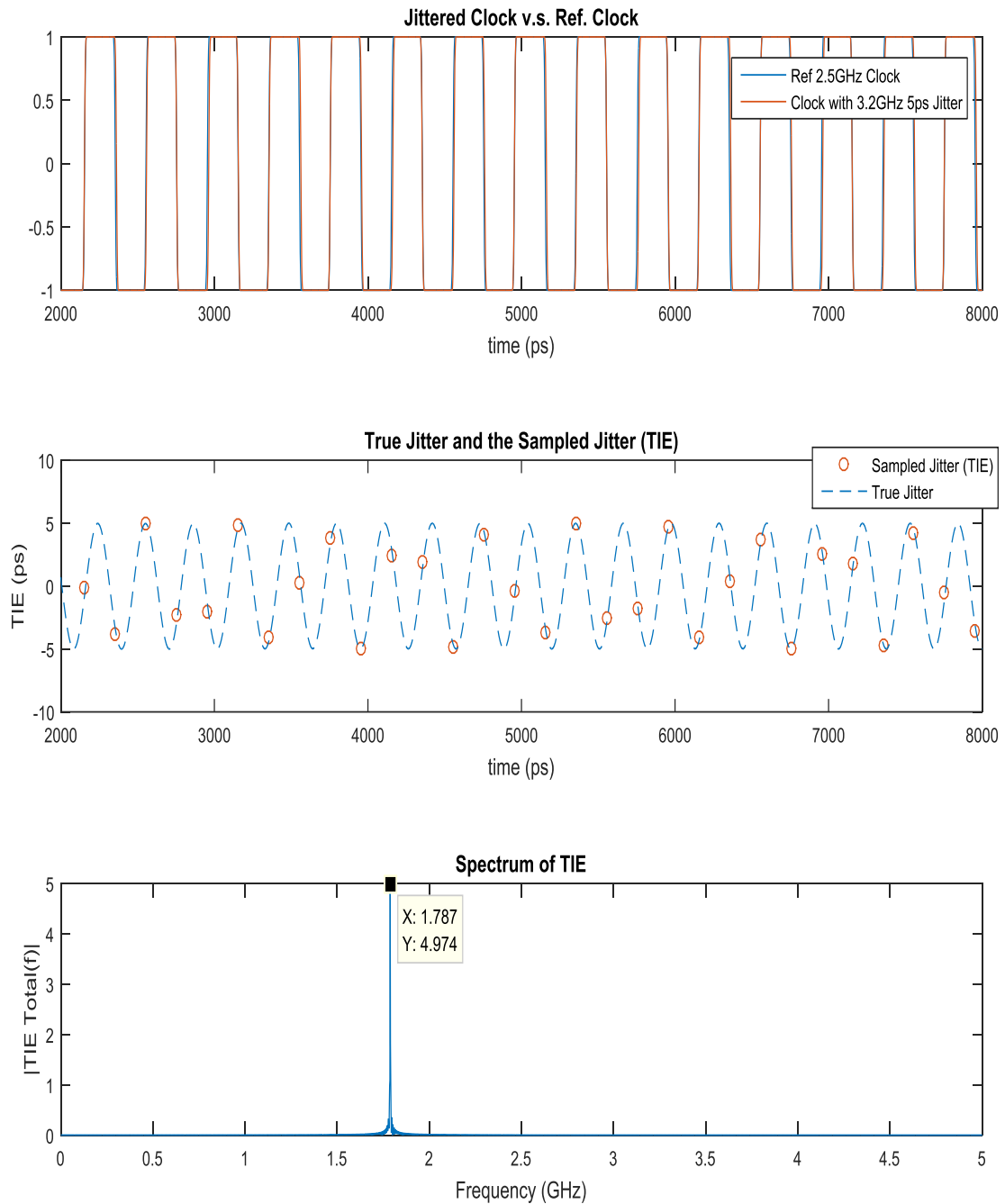
Figure 1.13. Under sampled case.

The under sampled case is showing a Nyquist frequency is 2.5GHz clock with a 3.213GHz periodic jitter. The jitter frequency is fast than the signal fundamental frequency. If connected the red circle of the sampled jitter, it doesn't close to the true jitter waveform. The TIE spectrum has confirmed that the 3.213GHz PJ has been transformed to a lower frequency jitter.

There is a relationship between the true jitter frequencies ω and the equivalent jitter frequencies ω' when jitter frequencies are larger than the signal Nyquist frequency.

$$\omega' = \alpha(2nf_0 - \omega) \tag{1.13}$$

$$where \quad \begin{cases} \alpha = 1 & (2n-1)f_0 < \omega \le 2nf_0 \\ \alpha = -1 & 2nf_0 < \omega \le (2n+1)f_0 \end{cases}$$
$$n = 1, 2, 3......$$

The expression has been verified using TIE spectrum; the following Fig.1.14 is comparing the equation calculated equivalent frequency with numerical TIE spectrum simulation result.
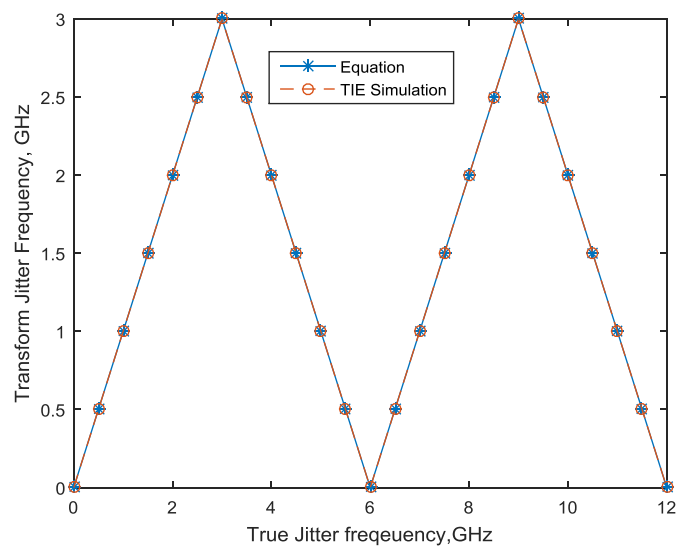
Figure 1.14. True jitter frequencies vs. transformed jitter frequencies.

1.4.2. PJ Amplification in a Clock Channel. In the section 1.4.1, a clock and

PJ frequency modulation mathematical derivation has been discussed. The signal

spectrum shows the physics more clear. In this example Fig 1.15 the clock data rate is

10Gbbops, which has 5GHz fundamental frequency.
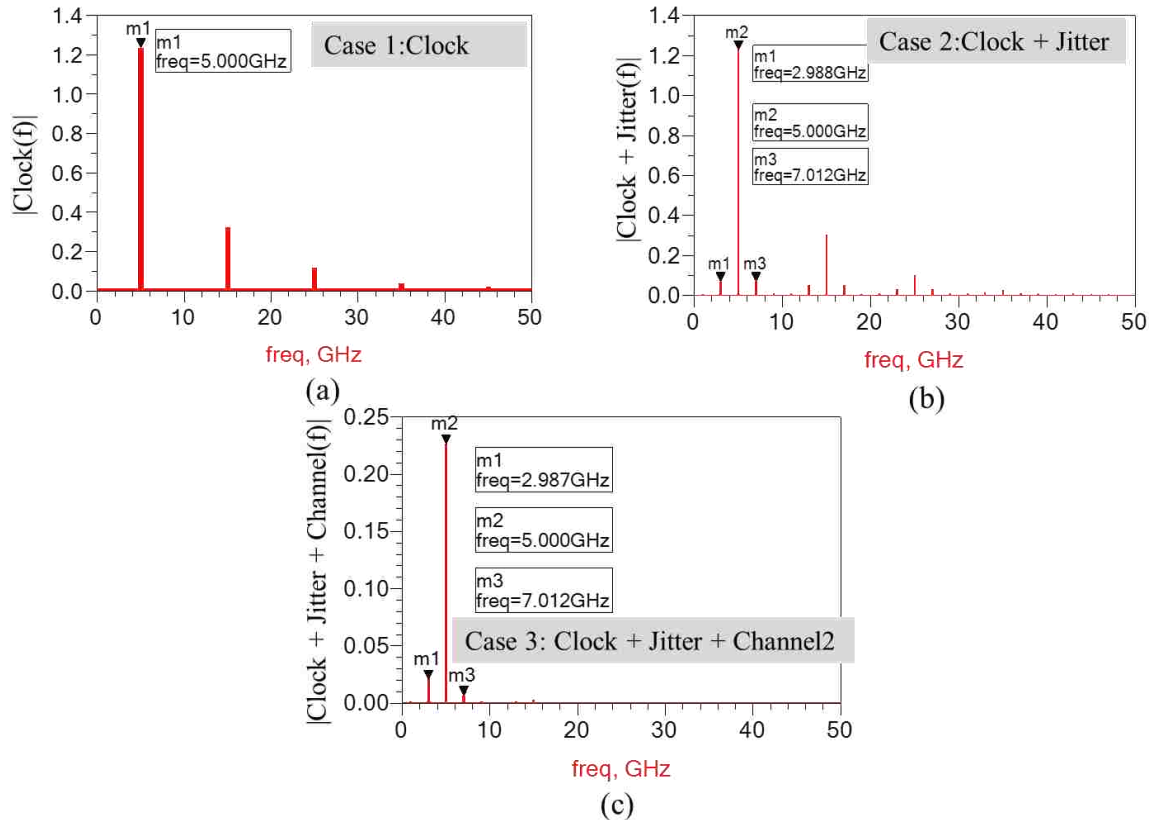
Figure 1.15. 5GHz clock and 2.121GHz PJ signal spectrum (a) Clock spectrum (b)
Clock+PJ spectrum (c) Clock+PJ spectrum after a lossy Channel.

The simulation is done by Agilent ADS channel simulation with 10000 bits. The

periodic jitter frequency is 2.012GHz. 5GHz clock fundamental frequency only have odd

harmonics in its spectrum as shown in the first figure. The second figure is showing the

phase modulation, there are two sidebands due to PM at the two sides of the clock

harmonics. The distance between the sidebands and the signal is $5 \pm 2.012\,\text{GHz}$.

The clock testing channels are shown in Fig. 1.16. Channel 1 is a lower loss

channel, which has about -14.7dB insertion loss at 5GHz. Channel 2 is higher loss

channel, and the insertion loss at 5GHz is about -18.9dB. The two different channel

losses have been used to show the channel loss impact on periodic jitter amplification.
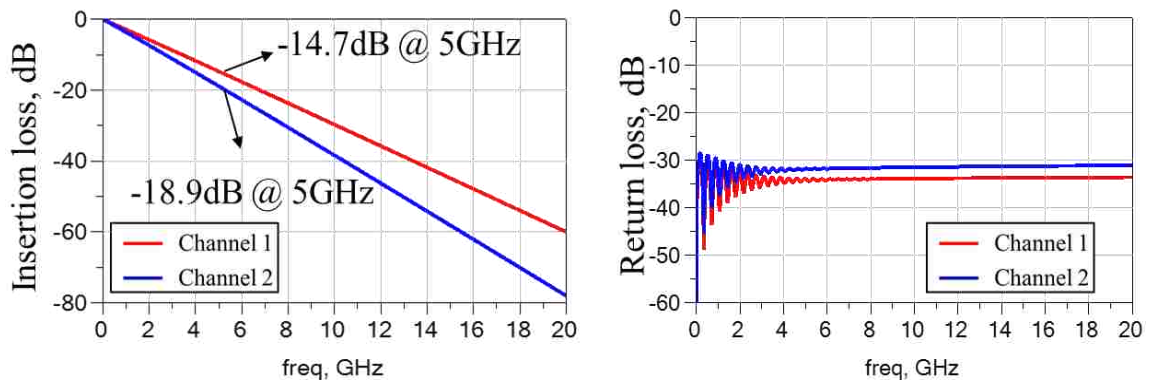
Figure 1.16. Two channel S Parameters.

In the ADS simulation, a periodic jitter with 5ps amplitude has been injected into

channel. The jitter frequency is varied. Fig. 1.17 is showing the output eye diagrams

density of channel 2 with a 10Gbps clock sources. They have been compared with the

input eye diagram (yellow dots) to show that the output jitter is increasing as the PJ

frequency increasing. The according jitter probability density functions are measured at

zero crossing and are also showing the same trend. In ADS, the output PJ's amplitude is

the time difference of the two peaks in the PDF. As shown in Fig. 1.17, the output (red

curve) PJ amplitude at 0.5 GHz is almost same as the input (blue curve). When PJ

frequency is 2, 3 and 4 GHz, output amplitudes are about 1.2, 1.5 and 2.2 times larger

than the input, respectively.
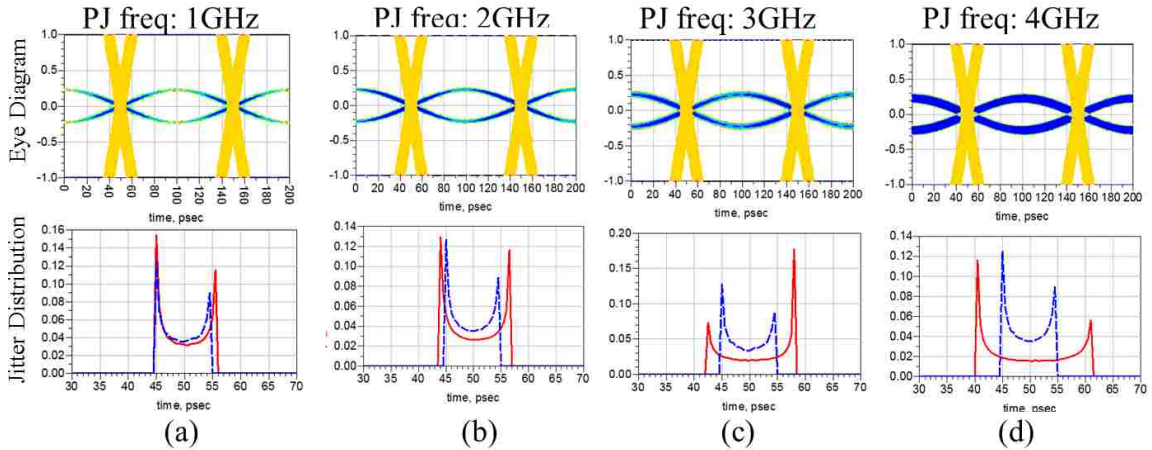
Figure 1.17. Eye diagrams and jitter distribution plots (a)1GHz PJ+5GHz clock (b)2GHz
PJ+5GHz clock (c)3GHz PJ+5GHz clock (d)4GHz PJ+5GHz clock.

Fig.1.18 shows output PJ amplification grows exponentially as Eq. 1.12 predicted,

and the predicted results have been compared with both ADS and TIE simulation. When

the channel loss is larger, the amplification is more significant
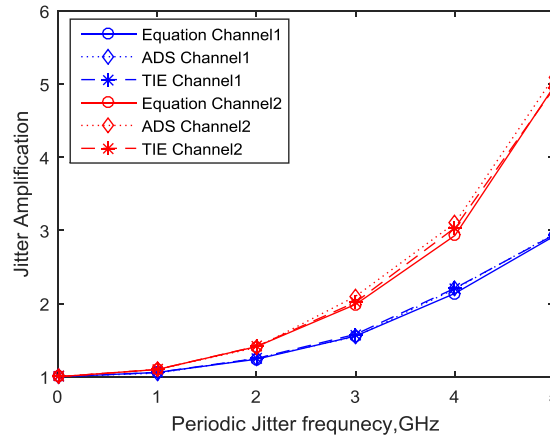
Figure 1.18. PJ amplification simulations vs. equation estimated value.

However, when we keep increasing PJ frequency, Eq. 1.12 will not continue correct predict the amplification. In this case, the jitter will be under sampled to a lower frequency jitter component. To obtain the correct amplification factor, people must use the equivalent jitter frequency. Eq. 1.13 describes the relationship between true jitter frequency and the equivalent jitter frequency. Substitute Eq. 1.13 into Eq. 1.12, then we have an equation for general PJ amplification Eq.1.14. The original Eq. 1.12 can only be used to estimate PJ amplification when jitter frequency is lower than clock Nyquist frequency.

$$
\begin{aligned}
F_{SJ}(\omega) &= \frac{1}{2}\left| \frac{S_{21}\left[f_0 + \alpha(2nf_0 - \omega)\right]}{S_{21}(f_0)} + \frac{S_{21}\left[f_0 - \alpha(2nf_0 - \omega)\right]^*}{S_{21}(f_0)^*} \right| \\
&= \frac{1}{2}\left| \frac{S_{21}\left[(1+2\alpha n)f_0 - \omega\right]}{S_{21}(f_0)} + \frac{S_{21}\left[(1-2\alpha n)f_0 + \omega\right]^*}{S_{21}(f_0)^*} \right|
\end{aligned}
\tag{1.14}
$$

$$
where \quad \begin{cases} \alpha = 1 \quad (2n-1)f_0 < \omega \le 2nf_0 \\ \alpha = -1 \; 2nf_0 < \omega \le (2n+1)f_0 \end{cases}
$$
$$
n = 1, 2, 3......
$$

Fig.1.19 shows the comparison of the equation predicted ADS simulated and TIE simulated amplification of two channels. The amplification curve shows than as the jitter frequency increasing, after the clock fundamental frequency, the amplification factor will decreasing exponentially. The amplification shows a periodic pattern, the period is the clock data rate. When PJ is at the fundamental frequency, the amplification is maximum.

PJ amplification as a function of PJ frequency and clock fundamental frequency is shown in Fig.1.20. PJ frequency is varied from 0.5GHz to 10GHz. The clock fundamental frequency is changing from 1GHz to 5GHz. The curves show that when PJ is lower than Nyquist frequency, amplification factor is insensitive to the clock data rate.

However after Nyquist frequency, data rate have a significant impact on the amplification factor.
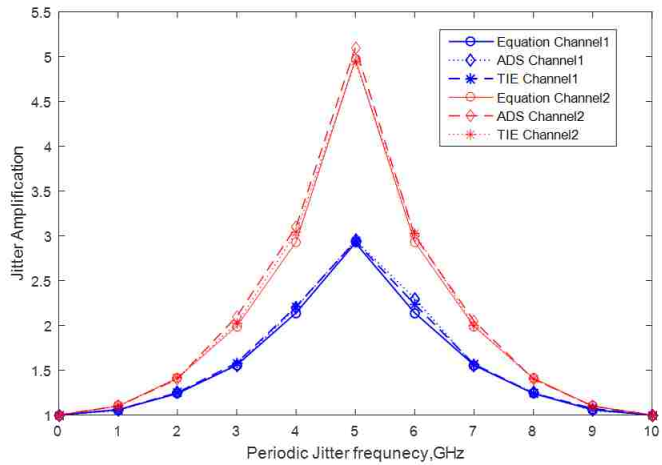
Figure 1.19. PJ amplification simulations vs. equation estimated value.
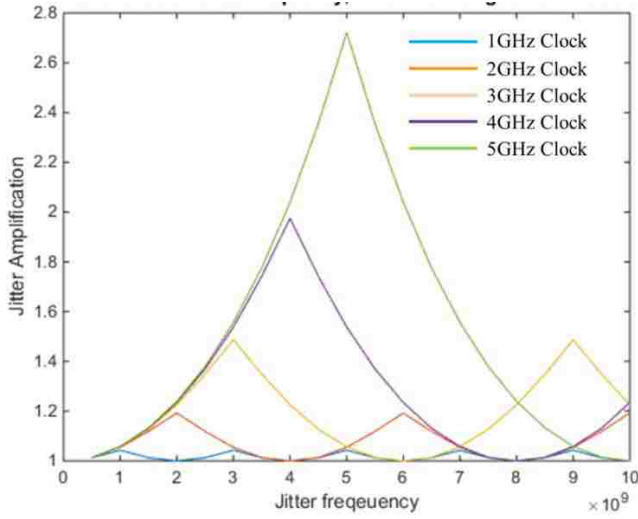
Figure 1.20. PJ amplification as a function of PJ frequency and clock fundamental frequency.

PJ amplification factor is also is scale with the channel loss. Fig. 1.21 is shown the PJ changing trend as the channel loss increasing at the fundamental frequency. When channel loss is about -5dB at 3.5GHz, the amplification is about 1.2. The amplification

can be almost ignored when channel loss is smaller than 5dB. However, when the channel loss is reach about -25 dB at 3.5GHz, the amplification become larger and more significant, which cannot be ignored.
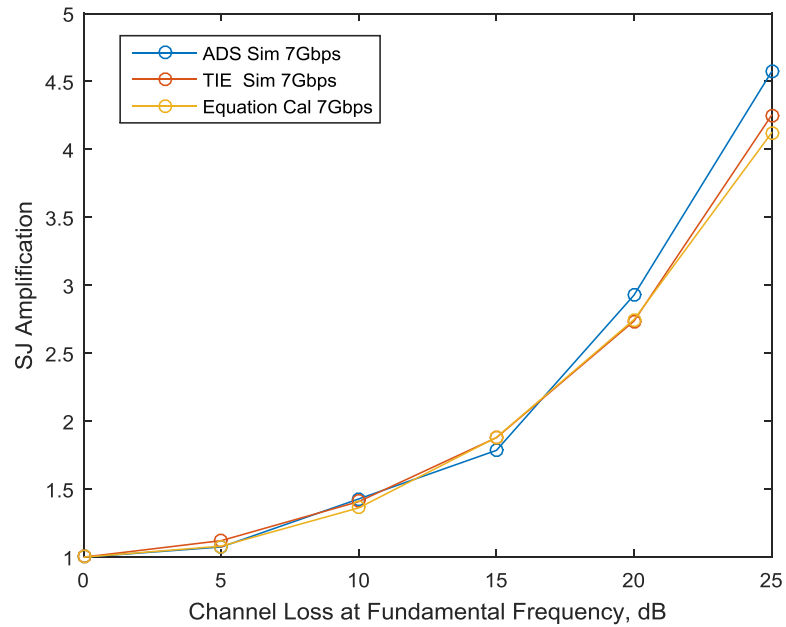
Figure 1.21. PJ amplification as a function of PJ frequency and clock fundamental frequency.

1.4.3. PJ Amplification in a PRBS Channel. PRBS channel spectrum has more frequency components compared to clock spectrum. Each PRBS harmonics will modulated with the PJ, therefore the frequency modulation result will more complex. Using a 10Gbps PRBS 3 as an example is shown in Fig.1.22, it only has harmonics at pattern frequency$\mathbf{f_0} = \frac{1}{\mathbf{T_0}} = \frac{1}{\mathbf{1/data\ rate}}$, and $\mathbf{f_{pat}} = \frac{\mathbf{f_0}}{\mathbf{2^3 - 1}}$. Due to phase modulation, each harmonic have two sidebands. After lossy channel, the spectrum components beyond the Nyquist frequency are heavily attenuated.
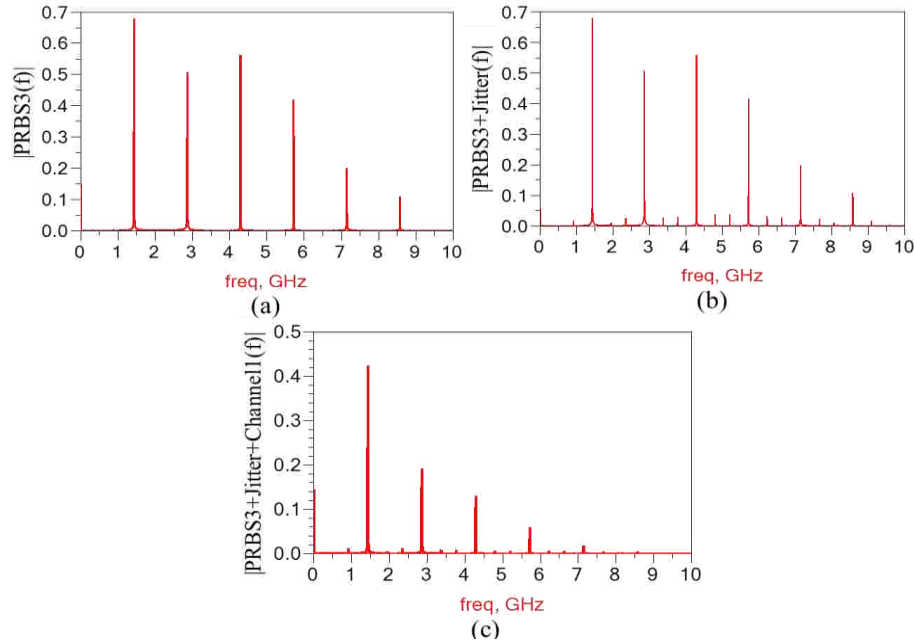
Figure 1.22. Signal spectrum of 10Gbps PRBS 3 with a PJ (a) PRBS3 (b)
PRBS3+0.512GHz PJ (c) PRBS3+0.512GHz PJ+lossy channel.

ADS simulation can't be used to verify or monitor jitter's changing trend, because

the ISI is dominant in this case. Therefore, the first step of using numerical method study

PJ amplification of PRBS channel is to do jitter separation and remove all the data

dependent jitter. The jitter separation details have been discussed in section 1.3.4.

When jitter frequency is smaller than all the harmonic frequencies, their

frequencies must be relative low. So the amplification isn't significant. The amplification

curve is shown in the Fig. 1.23.

When jitter frequency is larger than some of the harmonic frequencies, the

situation become more complex. Due to signal frequency component is very different, the

modulation terms become quite different. So the amplification shows a data pattern

dependent trend. Fig. 1.24 shows a same PJ's amplification in a clock, PRBS3, PRBS5

and PRBS7 channel with a same data rate 7Gbps, separately. They all show a periodic

pattern. And the amplification factor is largest in the PRBS7 channel. And the numerical

simulation results show that PJ is a data dependent jitter.

Figure 1.23. PJ amplification when PJ frequency is smaller than all the harmonics.

Figure 1.24. PJ amplification when PJ frequency is smaller than some of the harmonics.

1.4.4. Summary. The study and comparison shows that TIE can be used to monitor periodic jitter's changing trend of a passive channel after filtering the data dependent jitter. When the input jitter is a very low frequency jitter compared to the channel response time, the output is same as the input jitter. There is no jitter amplification. It can be treated as another rece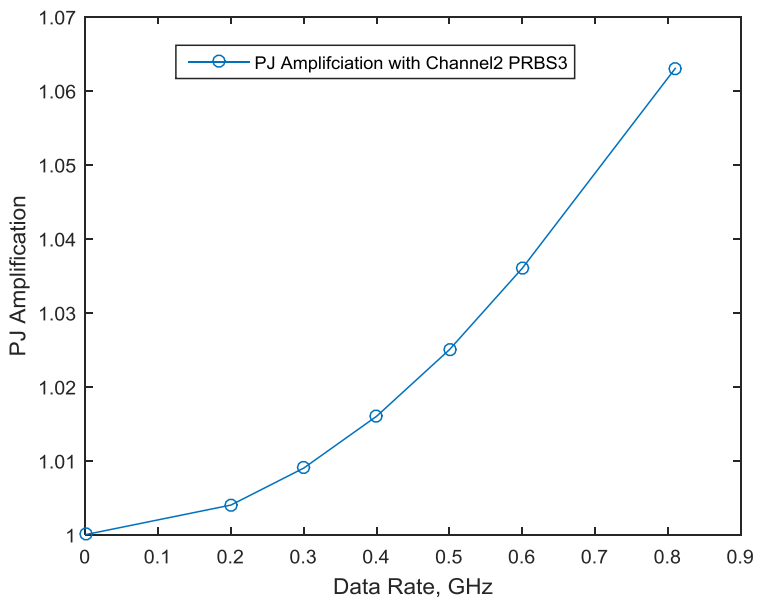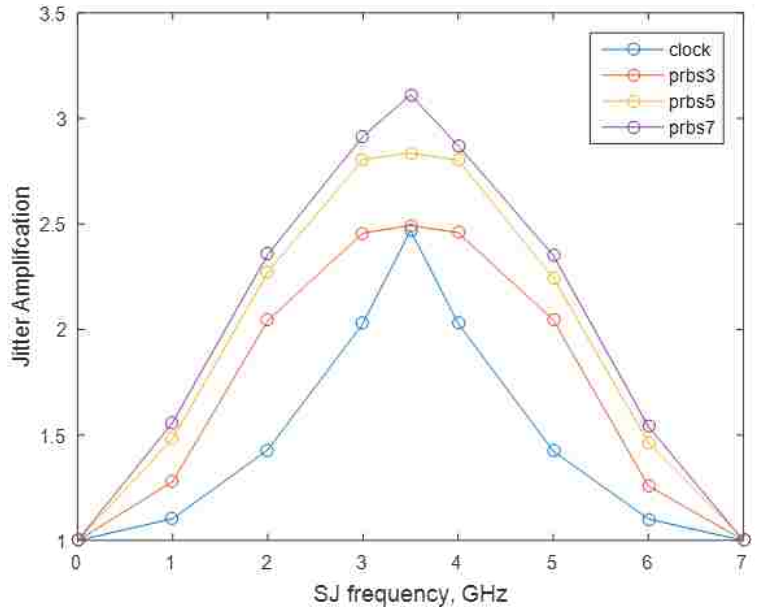iver random jitter. This assumption is widely used in many of statistical approaches. In addition, periodic jitter can be amplified by passive channel; however, the jitter amplification can be ignored for low loss channel. More specific, it mean when the channel loss is less than 5dB at the fundamental frequency, the amplification can be ignored. Overall, when periodic jitter frequency keeps increasing the amplification will show a periodic pattern. The similar trend can be seen in PRBS case.

1.5. RANDOM JITTER AMPLIFICATION

Random jitter amplification is defined as the ratio of the output to input standard deviations at the output to that at the input. It is important using the RJ's standard deviation or RJ's rms value as a value for quantifying RJ. Not as periodic jitter, RJ's peak to peak value is not a well-defined statistic value because RJ is unbounded. Its expected peak to peak value grows as the samples population increasing. Therefore the RJ's amplification is defined using standard deviation.

Clock channel jitter amplification has been verified in this chapter using TIE waveform. Then, RJ amplification in a simple data channel has been studied and also in a pseudo random data channel. The initial channel output waveform and the reference jitter free waveform is generated using Keysight ADS circuit simulation. The rest of post-

processing for obtaining TIE waveform is done be Matlab coding. The calculation results has been compared with published equations' calculated results.

1.5.1. RJ Amplification in a Clock Channel. To study the jitter amplification in a data channel, firstly, we need to verify the study procedure is correct. RJ amplification in clock channel has been simulated using TIE waveform method, and later on has been compared with ADS simulation result and equation calculated results. In the simulation, data rate is changing as 8, 12, 16 Gbps. Two different loss channels, as shown in Fig. 1.16, have been used as DUT (device under test). Fig.1.25 is shown the output eye diagram comparison of RJ with different data rate.
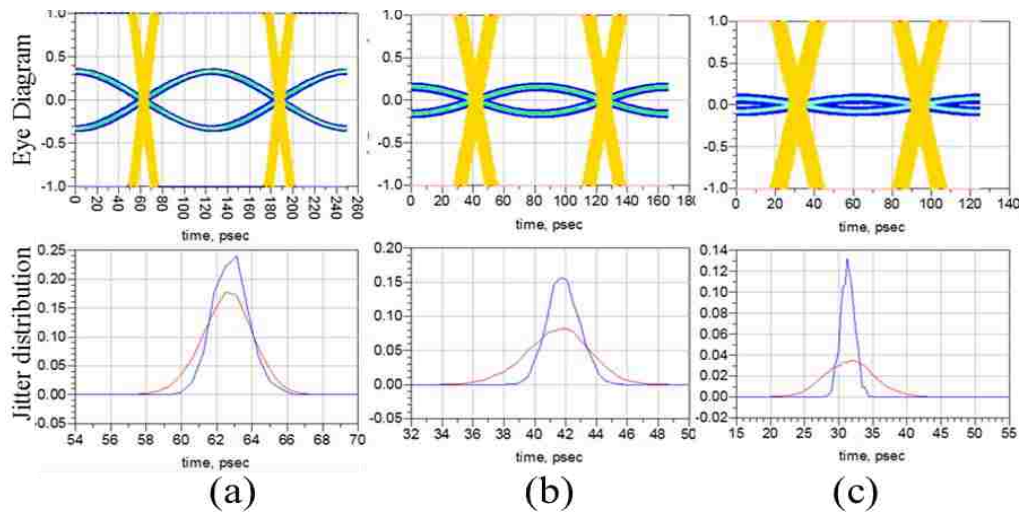

Figure 1.25. The output eye diagram comparison of RJ with different data rate.

Both eye diagram and jitter distribution clearly show that the output jitter has been amplified and it is growing as the data rate increasing. The signal spectrum in Fig.1.26 is shown the RJ modulation with signal. The strong spectrum components are all

signal spectrum. The RJ component is bandlimited white noise, it can be seen after zoom

in the spectrum below 6GHz (signal data rate is 12GHz).
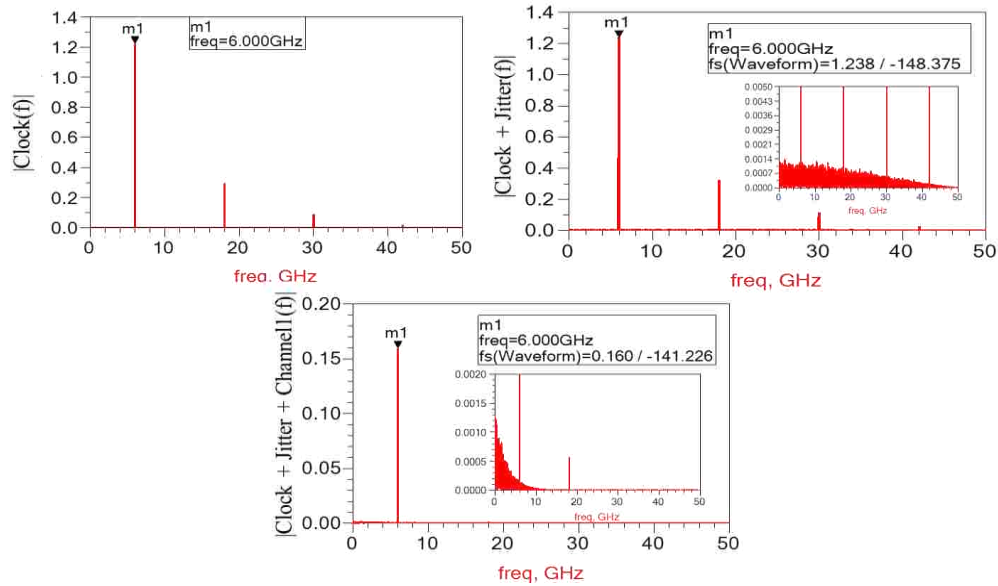
Figure 1.26. The signal spectrum when inject a 1ps RMS RJ.

The formulation used for correlation is based on paper. This method is modeling

RJ as an white noise, and then the averaged power can be obtained by the integration of

the power density (PSD) within the jitter Nyquist frequency, which equals ω_0 (signal

fundamental frequency).

$$F_{RJ} = \sqrt{\frac{1}{4\omega_0} \int_0^{\omega_0} d\omega \left| \frac{S_{21}(\omega_0+\omega)}{S_{21}(\omega_0)} + \frac{S_{21}(\omega_0-\omega)^*}{S_{21}(\omega_0)^*} \right|^2}$$ (1.15)

ω: jitter frequency

$\omega0$: signal fundament frequency

The simulation result is shown in Fig 1.27, and the simulation data rate is varied

from 4Gbps to 16Gbps. RJ amplification is growing exponentially as the data rate

increasing, and the three types of results are correlated well.

RJ amplification factor is also scale with the channel loss. Fig. 1.28 is shown the RJ changing trend as the channel loss increasing at the fundamental frequency. When channel loss is about -5dB at 7GHz, the amplification is about 1.3. The amplification can be almost ignored when channel loss is smaller than 5dB. However, when the channel loss is reach about -25 dB at 7GHz, the amplification become larger and more significant, which cannot be ignored

Figure 1.27. Output RJ amplification of the clock channel as the data rate changing.
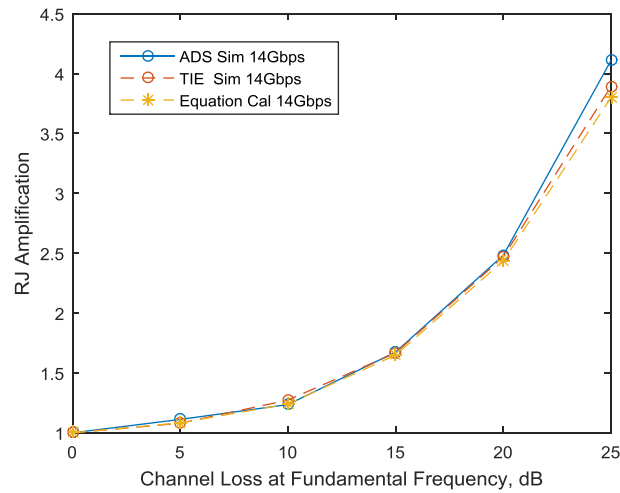
Figure 1.28. RJ amplification scale with channel loss of a clock channel case.

1.5.2.   RJ Amplification in a PRBS Channel. To monitor the PRBS jitter changing trend, same as PJ of a PRBS channel, after obtain the TIE waveform RJ needs to be separated with DDJ. RJ amplification is showing a similar trend as in clock channel, the amplification grows exponentially as shown in Fig.1.29. For the PRBS case, the RJ looks like isn't depending on data pattern. Therefore the amplification can be predicted using clock RJ analytical equation.
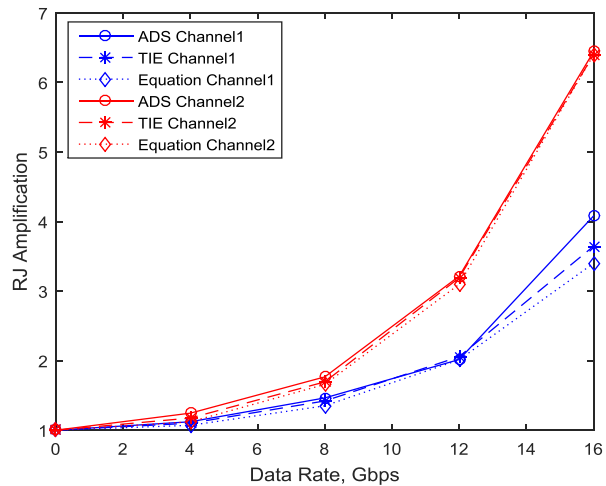

Figure 1.29. Output RJ amplification of a PRBS channel as the data rate changing.

RJ amplification scales with channel loss is shown in the Fig. 1.30.The channel loss is varied from -5dB to -15dB at the PRBS 7 fundamental frequency. The data rate is 7Gbps.
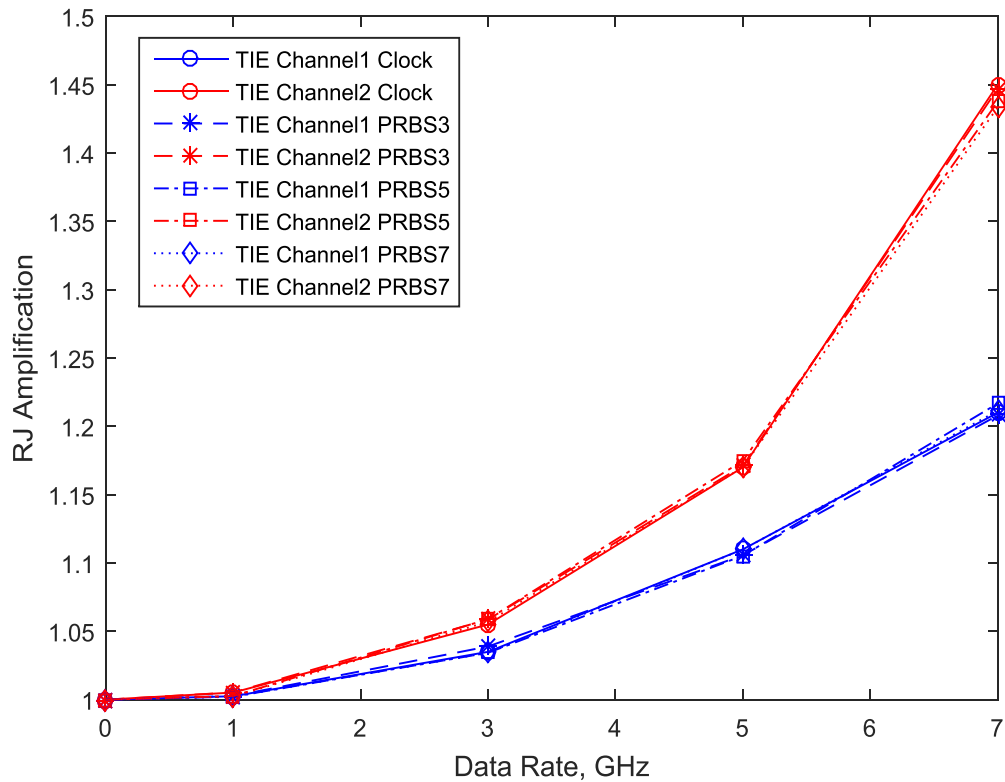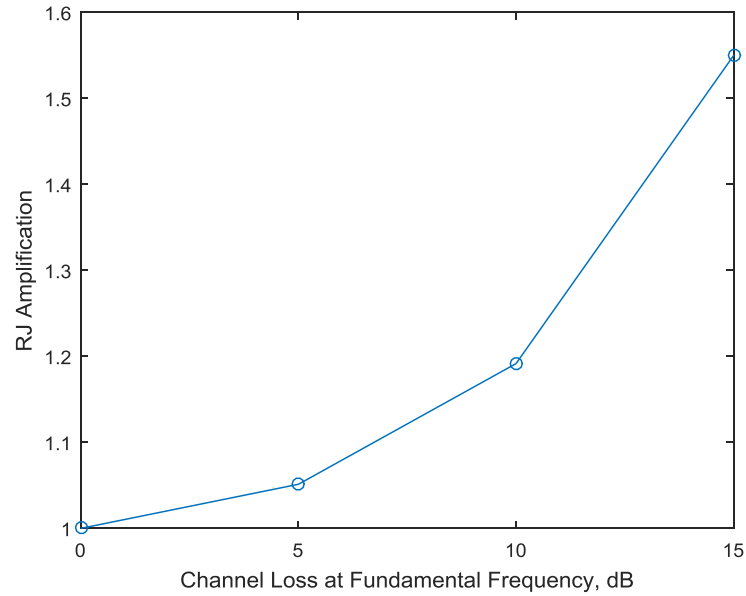
Figure 1.30. RJ amplification scale with channel loss of a PRBS7 channel case.

1.5.3.   Summary. The RJ amplification has been studied in this section. The study and comparison shows that TIE can be used to monitor random jitter's amplification trend. It is especially useful for the PRBS case, when there is DDJ and RJ component. TIE method can effectively remove the DDJ. Similar to PJ, RJ amplification grows exponentially and can be predicted using Eq. 1.14 and Eq. 1.15 in clock channel. Since the RJ is not data pattern dependent jitter, the amplification can be predicted using Eq.1.15. In addition, when the channel loss is less 5dB at the fundamental frequency the amplification can be ignored.

1.6. CONCLUSIONS AND FUTURE WORKS

PJ and RJ can be amplified in both clock and PRBS channels. The amplification is more significant concern in clock channel than it is in a PRBS channel. Also, the channel loss is another concern factor for the jitter amplification other than the data rate.

When the jitter frequency is low and the channel loss is low, both PJ and RJ amplification can be ignored. For the future work, a closed form analytical equation could be derived for the PRBS jitter amplification cases based in the current clock jitter amplification equation.

2. INVESTIGATION OF S21 MAGNITUDE EXTRACTION METHODOLOGIES USING A PATTERN GENERATOR AND OSCILLOSCOPE

2.1. ABSTRACT

S-parameter measurements of a digital link path are measured with VNAs or high-end TDRs. For multi-port in-situ measurements, these become inconvenient and time consuming. However, it can be handled more conveniently in the time domain (TD) by using a pattern generator and a multi-channel sampling oscilloscope, which are used for eye-diagram measurements. This paper outlines and compares three methods to extract S21 magnitude from the time domain measurements using a pattern generator and a sampling oscilloscope for any channel. The setup differs in terms of the input waveform and the processing. The comparison provides insight into the advantages and limitations of each method.

2.2. INTRODUCTION

S-parameters, used to characterize a channel, are usually obtained using Vector Network Analyzers (VNA), or can be extracted from TDT/TDR measurements. These expensive instruments are designed to obtain very accurate measurements up to several tens or even hundreds of GHz. Compared to conventional methods, the alternative way to obtain S21 using the pattern generator may be much cheaper than other S parameter measurement equipment. Multi-port in-situ measurements can also be handled more conveniently in the TD by using a pattern generator and a multi-channel sampling oscilloscope, which are traditionally used for eye-diagram measurements.

The difference between the proposed measurement and a VNA/ TDR

measurement setup is that the source is a digital signal and not accurately known. It does

not have a uniform spectral content and hence the choice of input waveform will

influence the accuracy and frequency range. There are several choices of inputs that can

be used but each of them will have their own drawbacks. As the digital waveforms are

not truly random or aperiodic, their spectrum will be discrete and will have nulls where

the signal energy content is low. These nulls correspond to the regions of bad signal-to-

noise ratio in the measurements. Three different input waveforms are used, and the

limitations in each case are studied to identify best measurement procedure for this setup.

This paper provides a methodology for S21 extraction from the TD measurements

of the channel. Nature of the spectral content of the used patterns will restrict the

accuracy of the S-parameters, as demonstrated using a sample DUT. Within limited

accuracy, S-parameters are obtained and compared to VNA measurements.

2.3. S21 EXTRACTION PRINCIPLE

2.3.1. Derivation. A two port network can be characterized using the Fig.2.1.

Figure 2.1. Two port network.

The terminal voltage of each port can be defined by the traveling wave as shown

in Eq.2.1. V_1^+ and V_2^+ is the incident wave of port 1 and port 2, V_1^- and V_2^- is the

reflected wave of port 1 and port 2. S_{21} can be defined as Eq.2.2,

$$V_1 = V_1^+ + V_1^-, \left.\begin{array}{c}\\\\\end{array}\right\}$$
$$V_2 = V_2^+ + V_2^-,$$

(2.1)

$$S_{21} = \left.\frac{V_2^-}{V_1^+}\right|_{V_2^+=0}$$

(2.2)

If the ports are matched on both sides with excitation at port 1, then S21 is same

as the voltage transfer function for this case, which can be described in Eq.2.3. Thus,

$$V_1^- = 0, V_2^+ = 0, \quad \text{and,} \quad S_{21} = \left.\frac{V_2^-}{V_1^+}\right|_{V_2^+=0} = \frac{V_2}{V_1} = H(j\omega)$$

(2.3)

2.3.2. Measurements for Obtaining S21. To obtain the S21 magnitude of the

channel using a pattern generator and sampling oscilloscope, V1, input voltage, can be

measured by directly connecting the pattern generator with the sampling oscilloscope.

V2, the output waveform, can be measured after passing the input through the DUT. Fig.
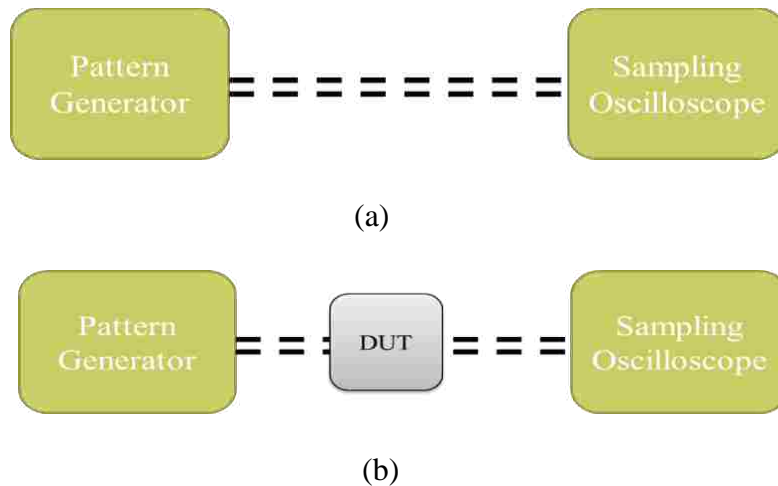
2.2 shows the setup of the two measurements.

(a)

(b)

Figure 2.2. Measurements setup for calculating S21 magnitude (a) Bypass measurement
for V1 at the oscilloscope side (b) DUT measurement for V2 at the oscilloscope side.

Due to pattern generator can generate different input signal, each signal spectrum will have its own features. So we create a series of tests according to different input signals. To obtain the voltage transfer function, we need two measurements.

2.4. APPROACHES

The pattern generator can be setup to provide pseudo random binary sequence (PRBS), or any user-defined bit patterns. Therefore, three different input waveforms are used. For defining the approaches, simulations have been developed by using circuit simulation software, Keysight Advanced Design System (ADS), and a 1 meter long 45 Ω transmission lines has been used as a DUT. Both setups are simulated in ADS transient analysis to observe the signal at the oscilloscope with a 50 Ω termination. The reference signal V_1 is obtained from the simulation for bypass measurement. The DUT output signal V_2 is obtained from the simulation for DUT measurement.

2.4.1. Using Data Pattern as Input. The complete procedure to obtain the S21 of the DUT is shown in Fig. 2.3. The input signal in this simulation is a PRBS 9 with 20 ps rise/fall time and 10 pattern repetitions. The data rate has been setup to 3.2 GHz. The simulated V1 and V2 are shown in Fig. 2.4. V2's waveform has about 5 ns delay due to the DUT's electrical length, which has to be removed before FFT, and this step has been repeated for the following two approaches. The measured voltage waveform will be truncated using a windowing function to enforce the start and ending value of the waveform to be same. This is to reduce the spectrum leakage when doing FFT. After FFT, the pattern harmonics has been picked up for the S21 calculation. The rest of the spectrum components will not be used.
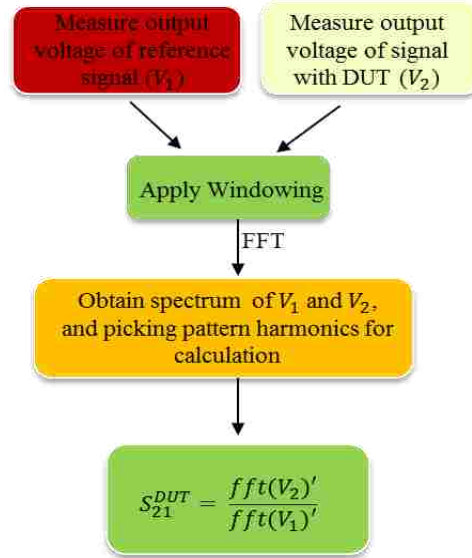
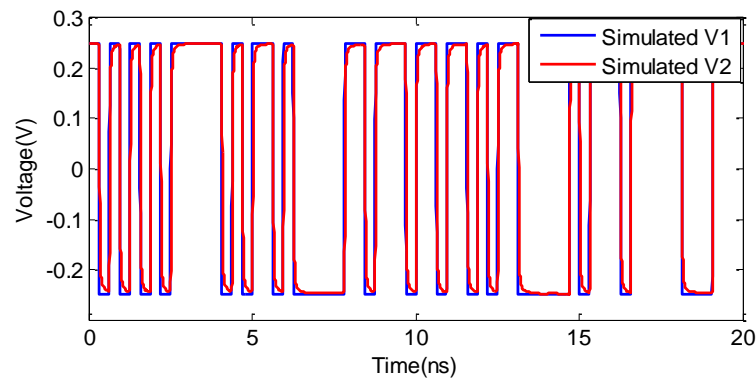Figure 2.3. S21 extraction procedure using data pattern as input.

Figure 2.4. V$_1$ and V$_2$ waveforms from ADS simulations for the first approach using PRBS9 as input signal.

After passing through the channel with ISI (inner-symbol interference), the signal is distorted. Then, the FFT function is used to convert both V$_1$ and V$_2$ waveforms from time domain to frequency domain. The spectrum of a PRBS waveform is discrete with the pattern harmonics and follows a sinc envelope which comes from the trapezoidal shape of the bits [8]. The pattern harmonics have been selected from both V$_1$ and V$_2$'s spectrum to calculate S$_{21}$, as the PRBS input signal spectrum is discrete with non-zero

38

energy only at pattern harmonics. At the frequencies where input signal itself has a zero or very low energy content, the signal to noise ratio (SNR) is very low leading to noise in calculated results[8]. Fig. 2.5 the red symbols show the pattern harmonics in the spectrum.
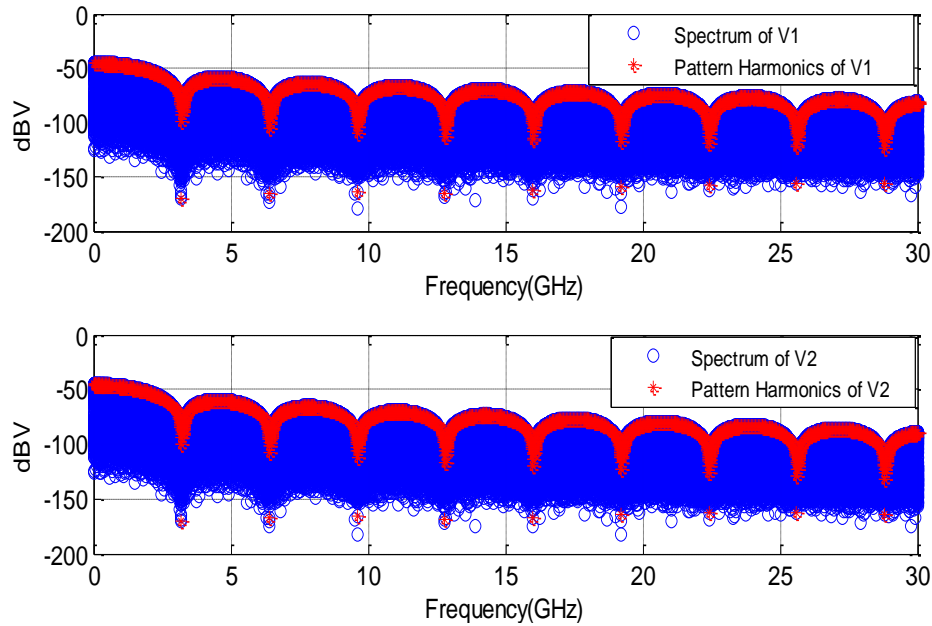

Figure 2.5. Simulated voltage spectra using PRBS9 as input signal.

The pattern harmonics under the sinc envelope can be located by finding the pattern frequency given as,

$$f_{pat} = \frac{f_0}{Pattern\ Length} = \frac{1/T}{Pattern\ Length} = \frac{Data\ Rate}{2^9 - 1}$$

(2.4)

The calculated S21 is shown in Fig. 2.6, where it is compared with the ADS frequency domain simulation result. The comparison shows a great agreement up to 30 GHz.
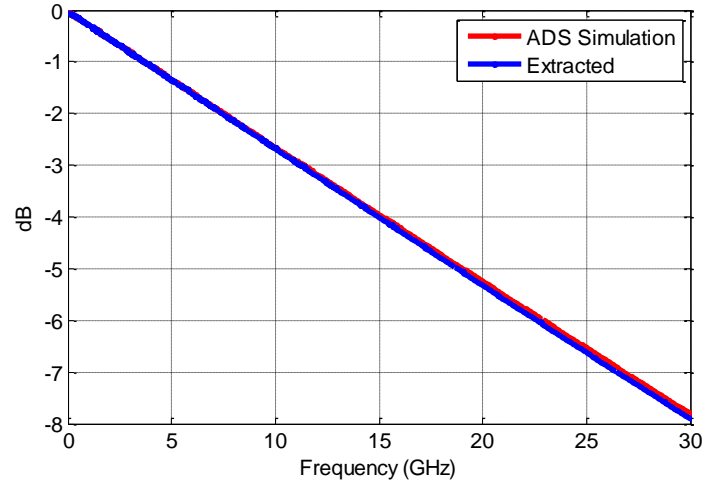
Figure 2.6. S21 comparisons between ADS frequency domain simulation result and extracted result using PRBS9 as input signal.

2.4.2. Using Clock as Reference Input. The second approach uses a clock waveform as the input signal. The data processing flow for this approach is shown in Fig.2 7. Clock frequency is 50 MHz and 10 periods as shown in Fig.2 8, which has 1 V peak to peak voltage, 50% duty cycle and 20 ps rise/fall time. A 5 ns time delay has been removed.
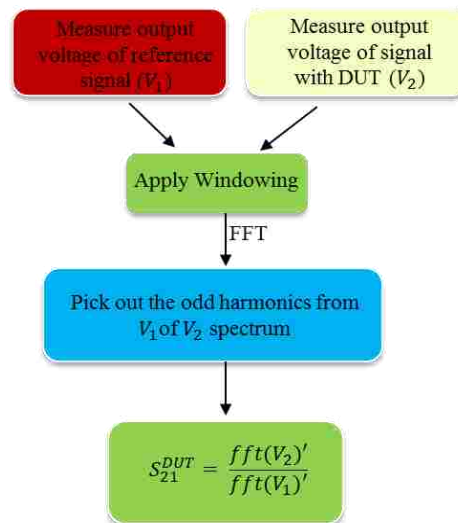

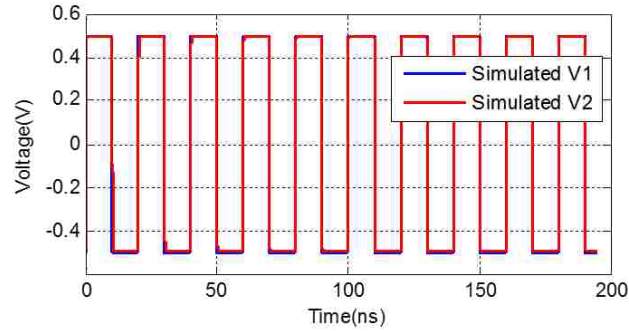Figure 2.7. S21 extraction procedure using clock as input.

Figure 2.8. V1 and V2 waveforms from ADS simulations for the second approach using a clock waveform as the input signal.

Similar to the first approach, the frequencies with low input signal energy content are identified, where a noise problem can occur due to low SNR. Thus, the S21 will be calculated by only using the odd clock harmonics in both simulated V1 and V2 spectrums. Fig. 2.9 shows about 80 dB differences between odd and even harmonics' magnitudes.
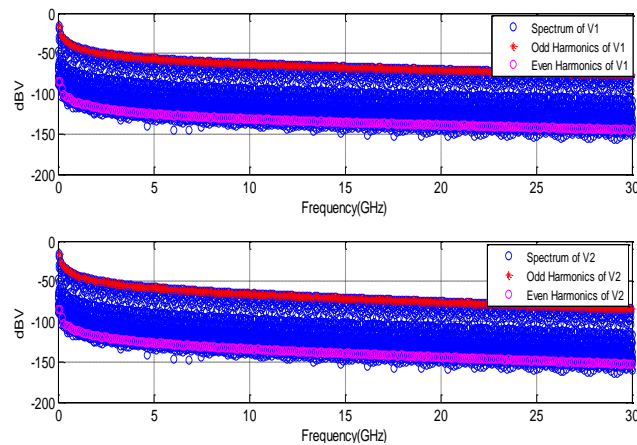

Figure 2.9. V1 and V2 spectrum using 50MHz clock signal as input.

The clock spectrum is constructed using odd and even harmonics, and for a 50% duty cycle clock, all the energy is carried on the odd harmonics. The even harmonics has

no energy. So to avoid picking the frequency domain component with bad SNR, we only use the odd harmonics to calculate the S21. However, if our input clock doesn't have perfect 50% duty cycle, then in certain frequency range the magnitude of even harmonics will raise up. There will cause issue since we are using only odd harmonics. The calculated S21 is shown in Fig. 2.10, which has been compared with ADS frequency domain simulation result.
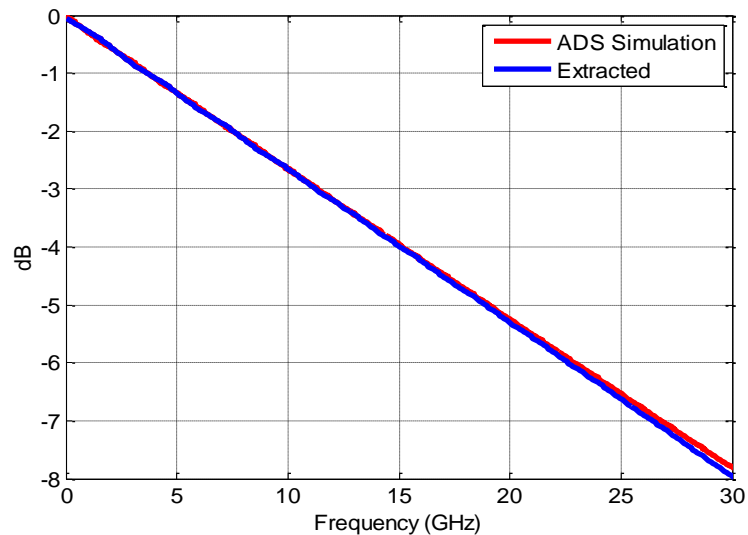

Figure 2.10. S21 comparisons between ADS frequency domain simulation result and extracted result using 50 MHz clock waveform as input signal.

2.4.3. Using TDT as Reference Input. The third approach is simulated using a clock waveform as the input signal. Frames of step waveforms are obtained by cutting both the V_1 and V_2 waveforms in time domain. The data processing flow is shown in Fig. 2.11. A 10 MHz clock has been used as shown in Fig. 2.12, which has 1 V peak to peak voltage, 50% duty cycle and 20 ps rise/fall time. Same as the above two approaches, a time delay of about 5 ns has been removed.
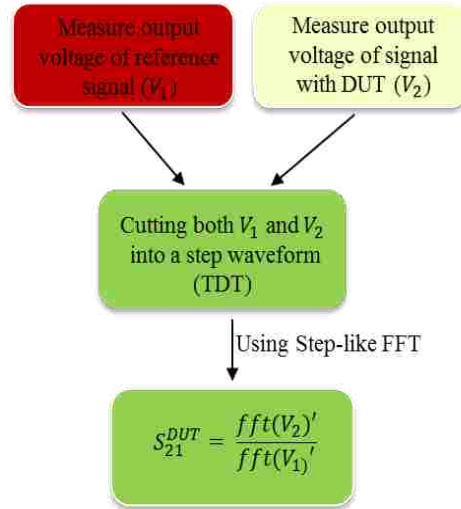
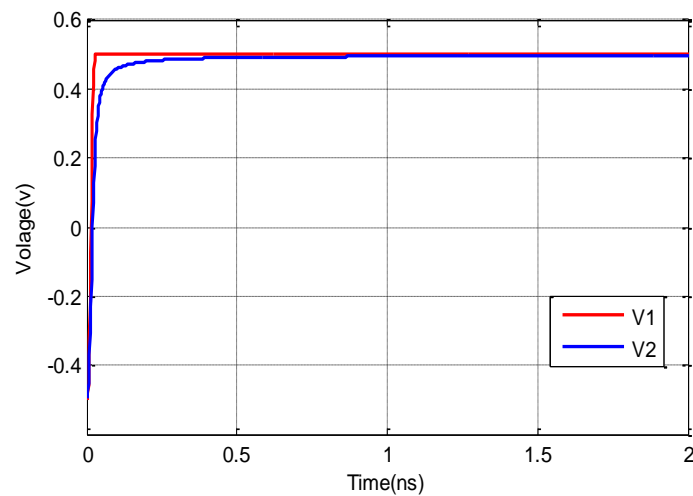Figure 2.11. S21 extraction procedure using a TDT waveform.

Figure 2.12. V_1 and V_2 waveforms from ADS simulations for the third approach using re-build TDT signals.

The spectrum is calculated by using a step-like FFT function [9], which has uniformly spaced dc and harmonics components. The step-like FFT function has ignored the incorrect even harmonics. The converted spectrums are shown in Fig.2.13. The calculated S21 is shown in Fig. 2.14, where it is compared with ADS frequency domain simulation result.
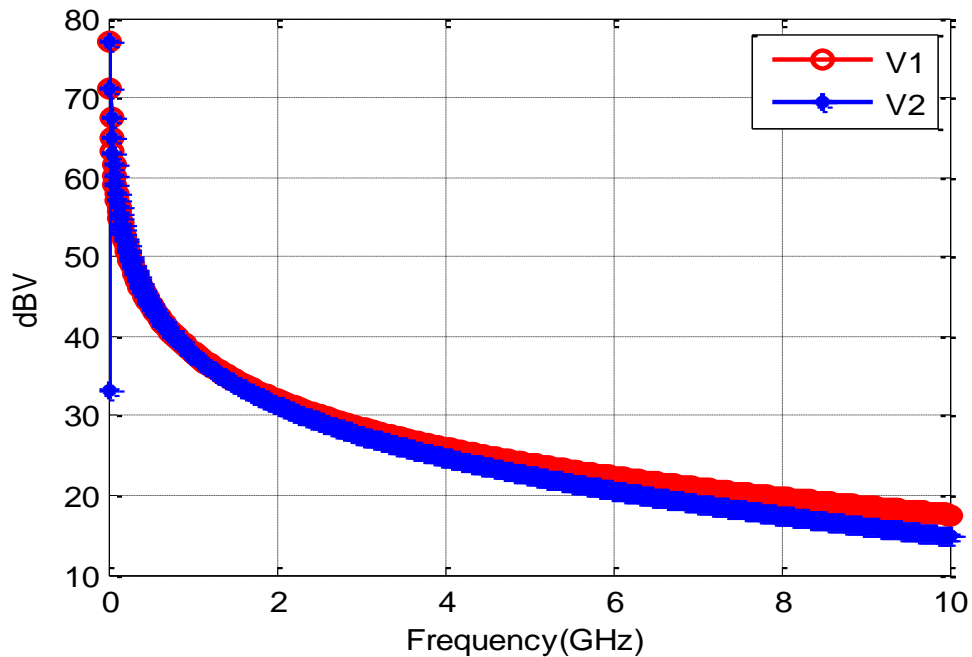
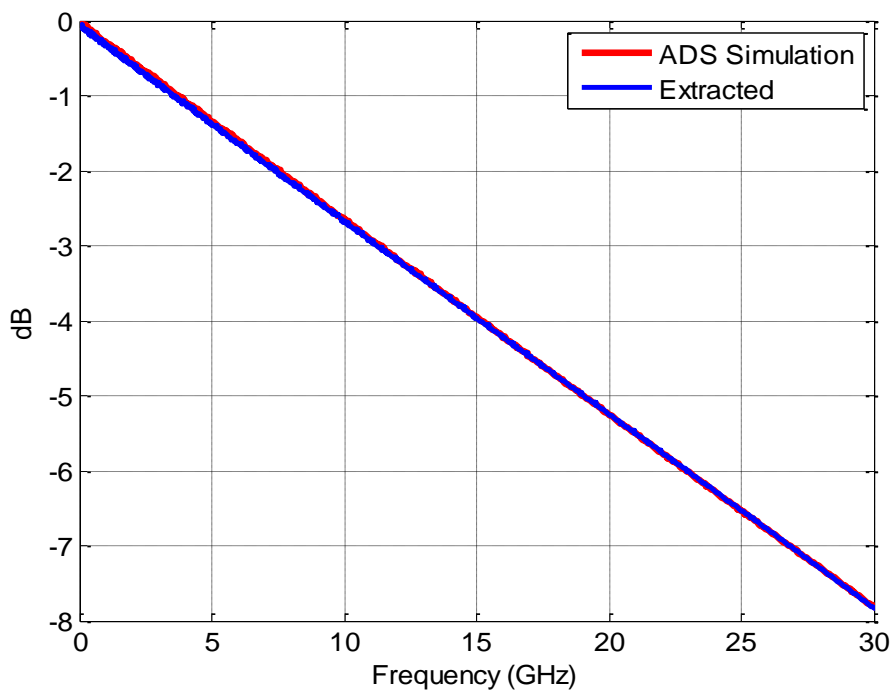Figure 2.13. V_1 and V_2 spectrums using the re-built TDT signals.

Figure 2.14. S21 comparison between ADS frequency domain simulation result and extracted result using re-built TDT signals.

2.4.4. Conclusion. All three methods have been compared together with the ADS frequency domain simulation result. The simulation results show that each source can be choose as an input for S21 extraction as long as using correct signal processing procedures. However, the simulation is only considering an ideal environment which no noise at all. This should be another concern for the real application. Fig.2.15 is shown the sS21 extraction approaches comparisons using ADS simulation. All three method will be validate using real measurement and compare with VNA measurement result in the next section.
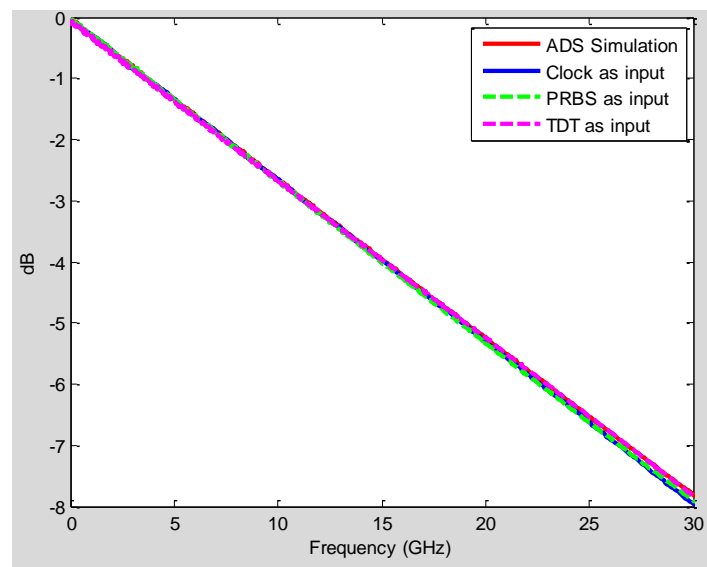

Figure 2.15. S21 extraction approaches comparisons using ADS simulation.

2.5. MEASUREMENTS

The three approaches are implemented using the setup shown in Fig.2.16. The bypass measurements are done by removing the DUT, and directly connecting the two cables.

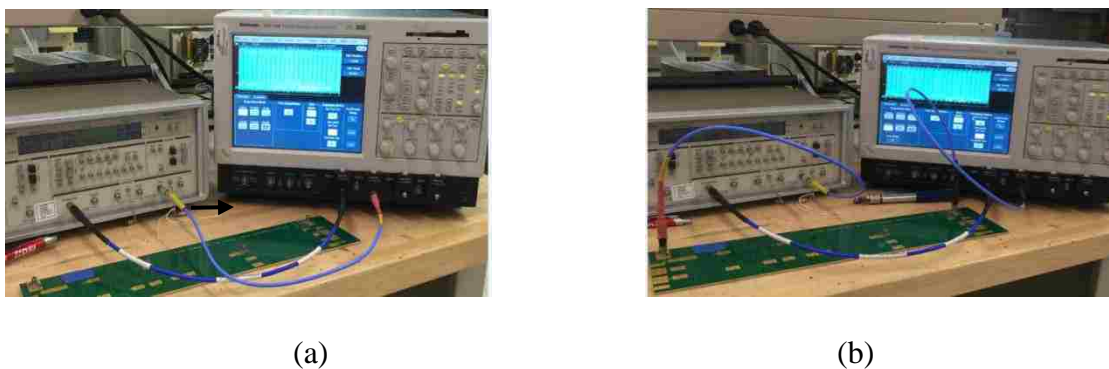   (a)   (b)

Figure 2.16. Measurements steps (a) V1 Measurement Pattern Generator + Cable1+Scope;(b) V2 Measurement Pattern Generator+ Cable1+PCB+Cable2+Scope.

The input signal for the three measurements has same 2 volts peak to peak voltage. Both input and output waveform has been averaged 10000 times for reducing the random noise in the measured data. To avoid the loosing connection caused by BNC connections, the Microwave Logic GigaBert 1400 Mb/s BERT generator and Tektronix TDS7404 Digital Phosphor oscilloscope with SMA connections has been picked to process the measurements as shown in Fig 2.17. VNA-measured S-parameters for the same DUT are used as the reference. About 1.4 ns delay, caused by the DUT, has been removed from V_2 for all three methods. The VNA measurement setup has been shown in Fig.2.18.
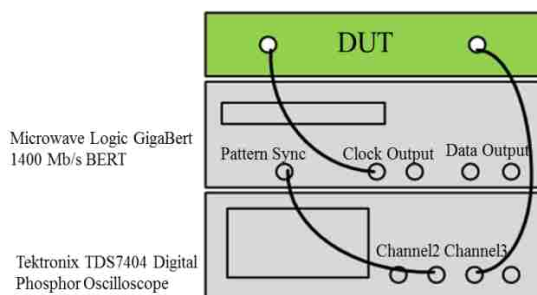

Figure 2.17. Measurement setup using a pattern generator and a digital oscilloscope triggered with the pattern sync output from the pattern generator.
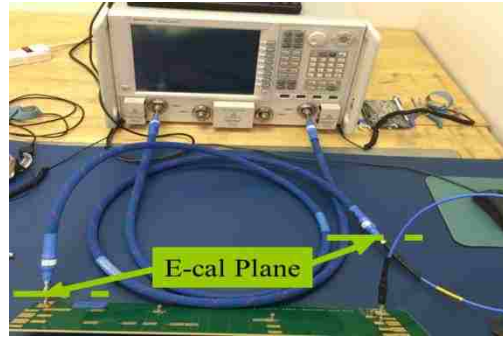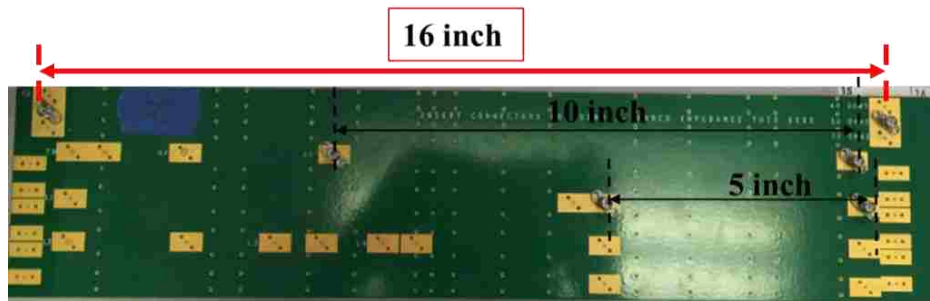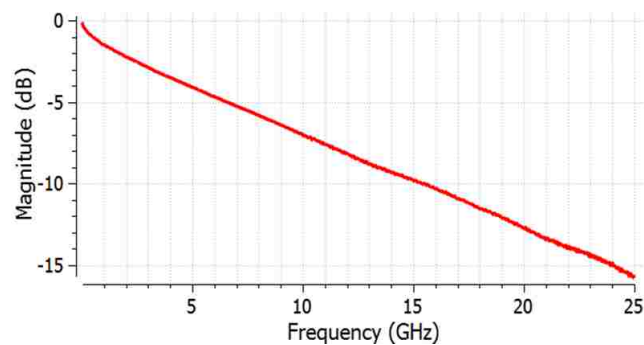
Figure 2.18. Measuring S-parameter of PCB + Cable 2.

Experiment DUT is low loss 50 Ohm PCB board, the trace length is about 16 inch as shown in Fig 2.19 (a). The measured S21 has a loss about 15dB up to 25GHz as shown in Fig 2.19 (b).

(a)

(b)

Figure 2.19. Measurement of reference S-parameter (a) PCB with 16inch trace (b) measured S21.

2.5.1. Measurement Cases. To compare the measurement results with different noise situation, three tests cased has been developed. In the measurement setup, the major noise is come from the mismatch at the pattern generator and oscilloscope connections. The following three test cases in Fig. 2.20 have been used to step by step reduce the possible noise sources in the real measurement. 6dB attenuator has been chosen to add between the connections of the instruments and the cables for blocking the reflection.
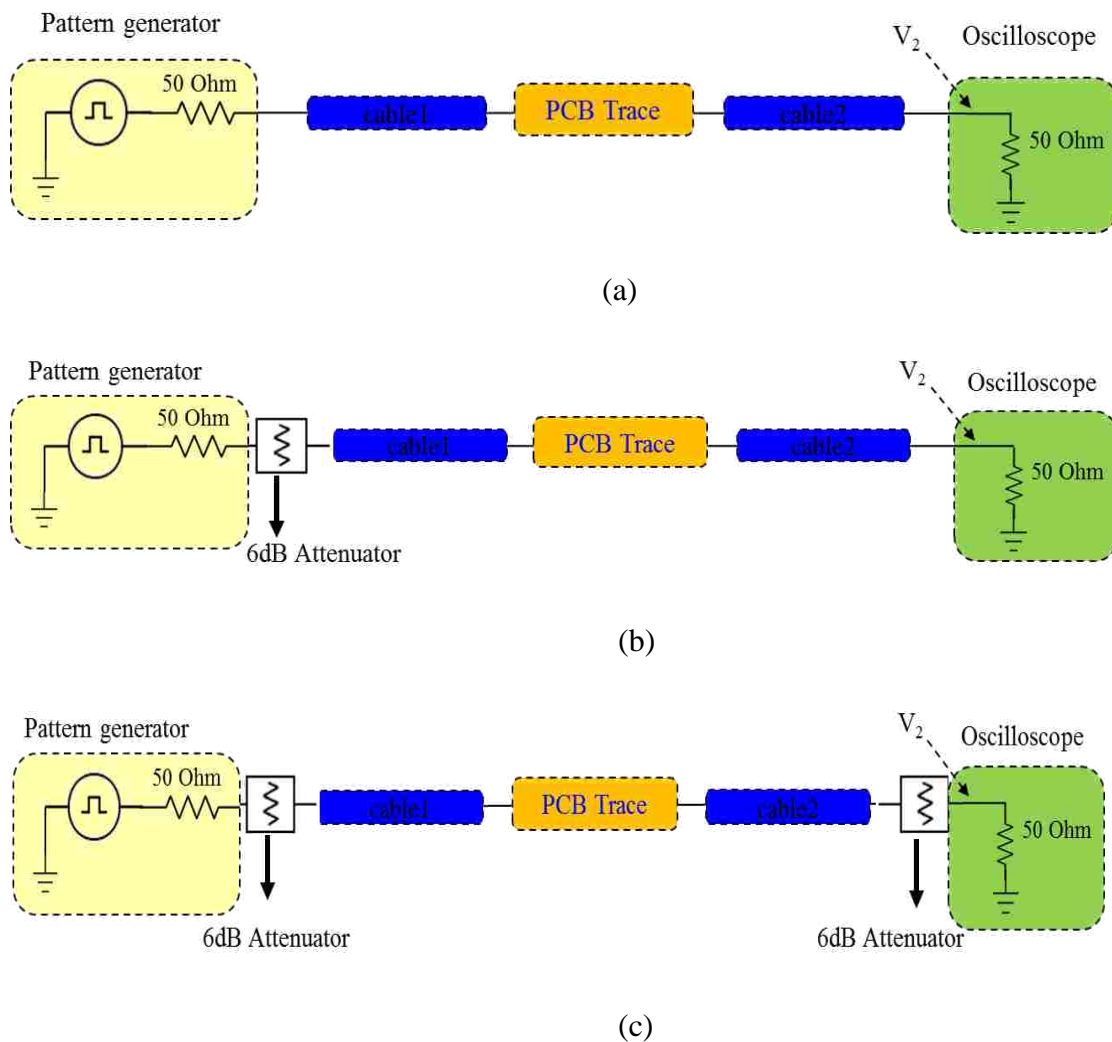

(a)

(b)

(c)

Figure 2.20. Different measurement cases (a) case1: no attenuator (b) case 2: with attenuator at pattern generator side (c) case 3: with attenuator at both pattern generator and scope side.

2.5.2. Using PRBS7 as Input. The bandwidth of the measured data has been limited by the first null at the data rate frequency. The random noise has overwhelmed the data at the null region. As the fastest data rate of Microwave Logic pattern generator is 1.405 GHz, it will be the maximum bandwidth for this study, to avoid the nulls from the data rate. Fig. 2.21 is measured time domain waveform, the signal shows large reflection. Their according frequency domain plots are shown in the Fig. 2.22, it shows the location of the nulls.
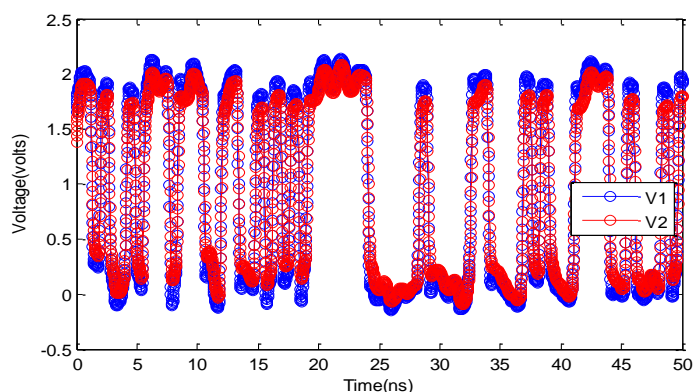
Figure 2.21. PRBs time domain waveform.

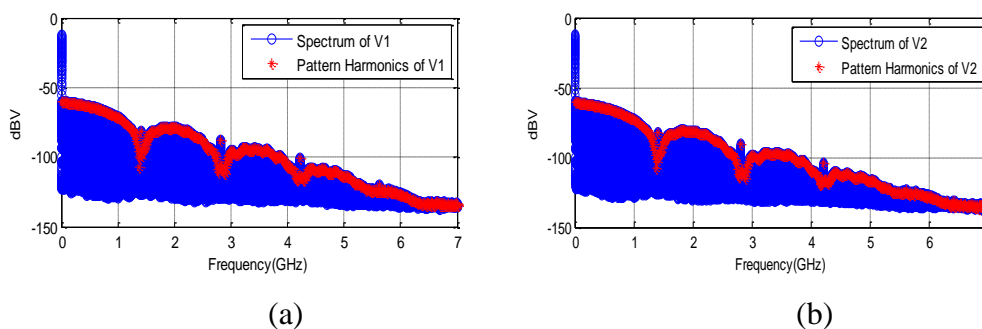|	
(a)	(b)

Figure 2.22. PRBs frequency domain plots (a) V_1 (b) V_2.

The calculated S21 magnitude is shown in Fig. 2.23. The overall magnitude level is matches the VNA measurement result. All three measurement cases has been

compared with VNA results, attenuators effectively reduced the noise in the system.

However, the calculated S21 is still noisy. As we expected, at the null frequency from the

data rate, 1.405 GHz approaches the effect of noise on the calculated S21 leads to

significant error. The second null has even lower signal strength, which leads to even
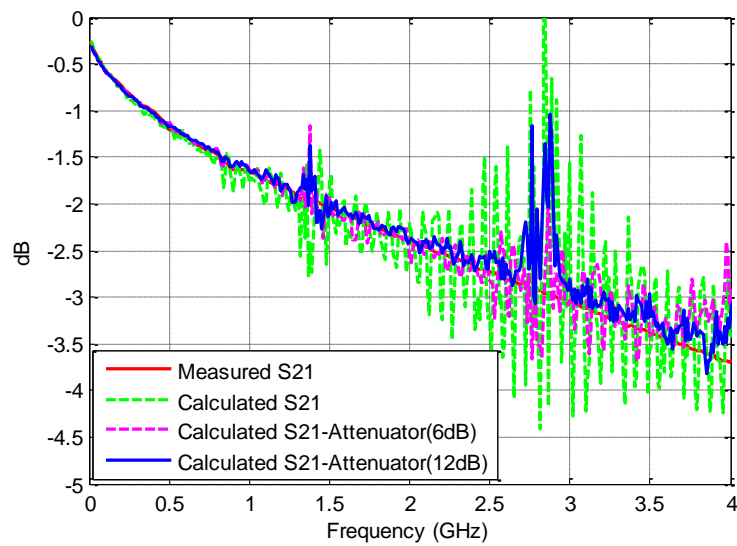
bigger error.

Figure 2.23. Extracted S21 using PRBS source.

2.5.3.   Using Clock as Input. In this measurement data, as the generated clock

does not have a perfect 50% duty cycle, the sinc envelope is very sensitive to the clock

duty cycle tha t can be described as[10],

$$|c_n| = \frac{A\tau}{T} |\frac{\sin(n\pi\tau)}{n\pi\tau/T}||\frac{\sin(n\pi\tau_r/T)}{n\pi\tau_r/T}| \tag{2.5}$$

The discrete Fourier Transform spectrum magnitude can be expressed by the

expansion coefficient as Eq. 2.5. The clock duty cycle is expressed as τ/T, which is

related to the sinc envelope. When the clock signal is exactly 50% duty cycle, the even

harmonics (when n = 2, 4, 6…) are all zero. However, when the duty cycle has a small

variation from an exact 50%, it can cause the even harmonics' levels to vary widely, and

these levels will overwhelm the odd harmonics' level. Therefore, the bandwidth has been

limited by the crossing frequency region of the even and odd harmonics. Fig.2.24 is

shown the measured time domain waveform. Fig. 2.25 shows the magnitude of the odd

harmonics.

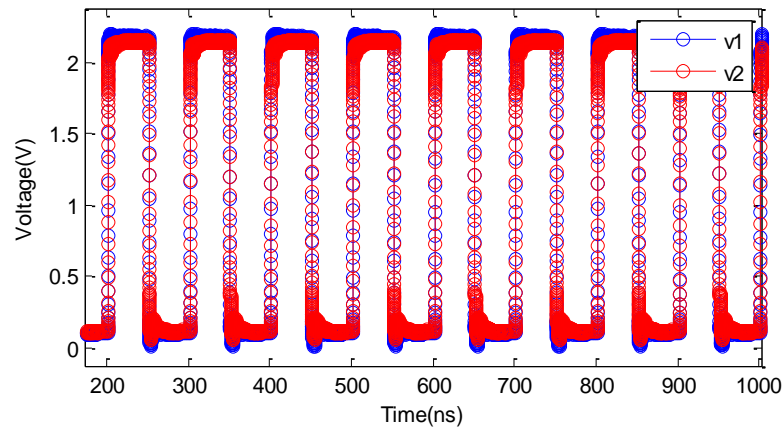Figure 2.24. Clock time domain waveform.

(a)   (b)
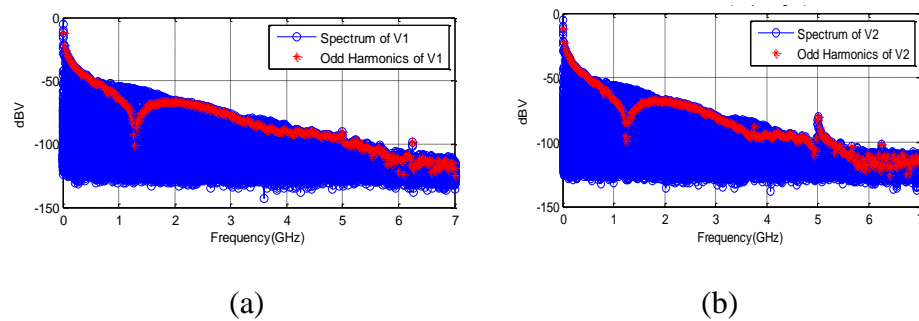
Figure 2.25. Clock frequency domain plots (a) V_1 spectrum (b) V_2 spectrum.

The calculated result is shown Fig. 2.26, and it has a lot of noise along the

frequency range, and with about 0.1 dB magnitude difference compare to VNA measured

result. Due to the bad SNR at the even and odd harmonics cross-region, the calculated S21 is significantly off from the VNA measured result. The data with two attenuators at the two sides is the best result, which indicates that the mismatch at the two side of the measurement setup is the major concern.
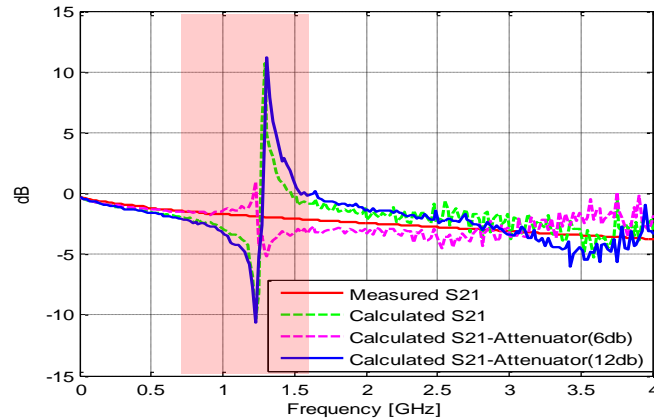
Figure 2.26. Extracted S21 using clock source.

2.5.4.   Using Step Signal as Input. In this measurement data, a 10MHz clock has been used as input. The entire recorded clock time length is 1 μs with 10 periods, and both measured V1 and V2 has been cut to 50 ns to create the re-build TDT signals. The calculated spectrum using step-like FFT function is shown in Fig. 2.27.

(a)   (b)

Figure 2.27. TDT signals (a) time domain waveforms (b) frequency domain waveforms.

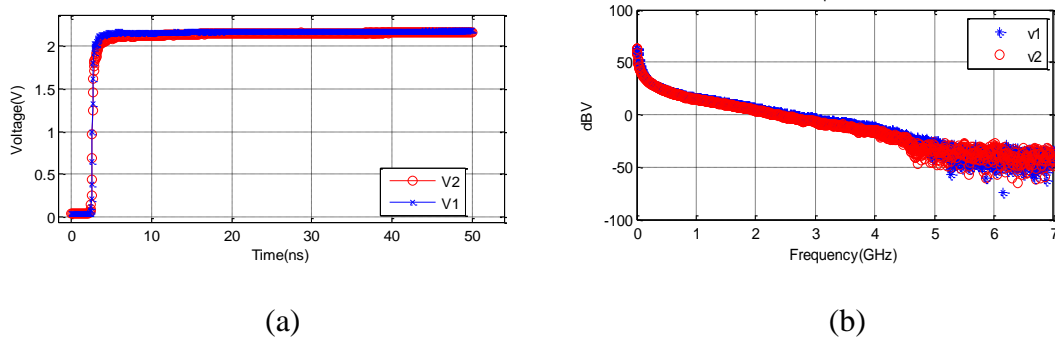The calculated result is shown Fig.2.28, and it shows that this approach has also been affected by the mismatch in the system compared to the VNA measured result. The attenuator can help reduce the reflection, but it cannot completely remove the noise.

Figure 2.28. Extracted S21 using TDT source.
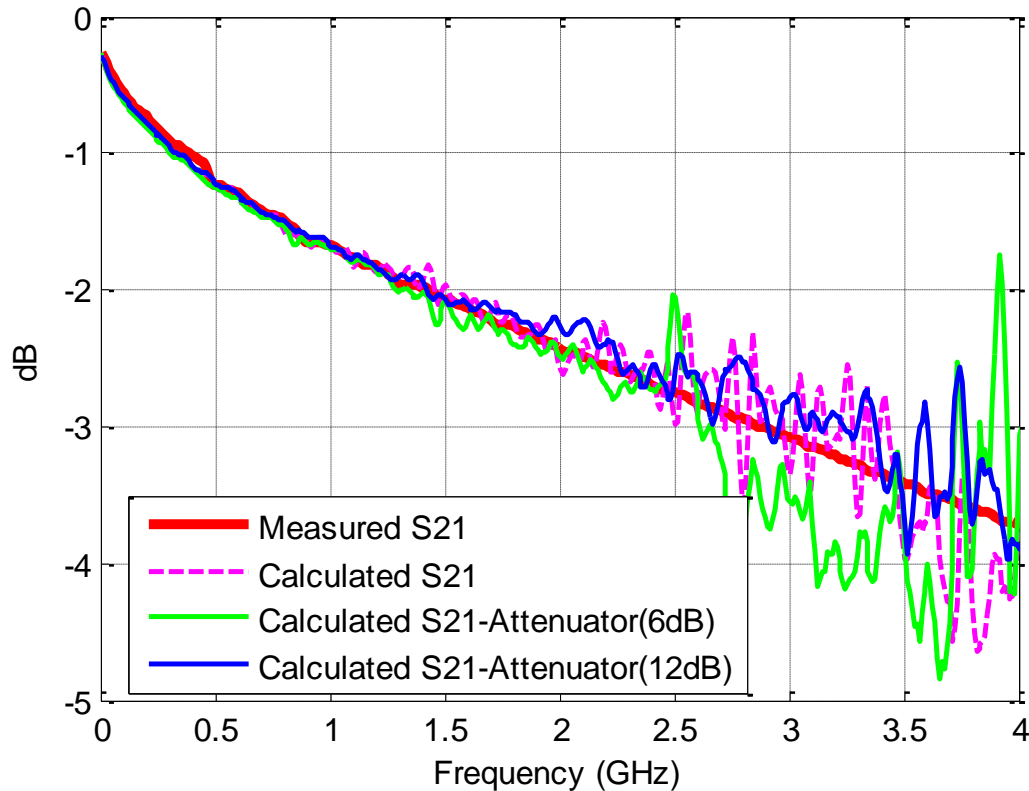
2.6. CONCLUSION AND FUTURE WORK

In this chapter, three approaches have been compared for extracting S21 magnitude using a pattern generator and an oscilloscope. The three approaches extracted S21 results have been compared with VNA measured results in Fig.2.29. To obtain the accurate S21 results, there are some considerations have to be noticed before choose each method.
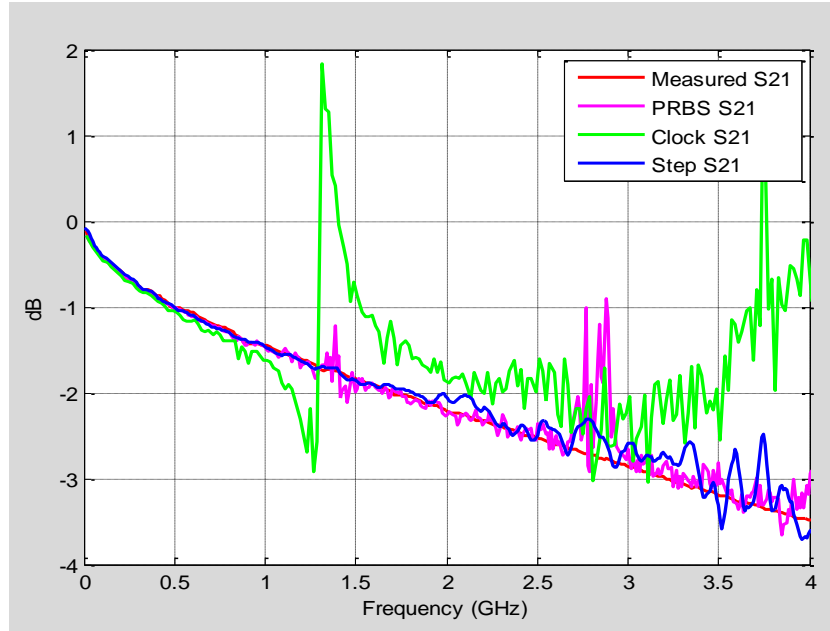
Figure 2.29. Extracted S21 comparison.

- Using PRBS Source

    - S_{21} bandwidth is limited by the data rate;

    - To obtain a good result, we need a high speed pattern generator.

- Using Clock Source

    - The clock duty cycle would be a limitation of the S_{21} bandwidth;

    - To obtain a good result, we need a precise 50% duty cycle clock.

    - Using Step Source

    - In step source case, we only need a fairly slow clock to obtain enough resolution in the frequency domain.

In addition, in all three methods, we need the scope bandwidth large enough to achieve the required bandwidth. The three approaches will be tested using other signal generators and oscilloscopes in the future. Since our current rise time is not fast enough,

so we may have weak power at the transmitter side beyond certain frequency. Therefore the future work will also need a signal generator with faster rise time.

BIBLIOGRAPHY

[1]   Chaudhuri, Santanu, et al. "Jitter amplification characterization of passive clock channels at 6.4 and 9.6 Gb/s." *2006 IEEE Electrical Performane of Electronic Packaging.* 2006.

[2]   Madden, Chris, et al. "Jitter amplification considerations for PCB clock channel design." *Electrical Performance of Electronic Packaging, 2007 IEEE*. IEEE, 2007.

[3]   Rao, Fangyi, and Sammy Hindi. "Frequency domain analysis of jitter amplification in clock channels." *Proc. IEEE 21th Topical Meeting on Electric Performance of Electronic Packaging, Tempe, AZ.* 2012.

[4]   Martin Miller. "Understanding Apparent Increasing Random Jitter with Increasing PRBS Test Pattern Lengths." *DesignCon, Santa Clara, CA*. 2013.

[5]   Chang, Yu Sam, Dan Oh, and Chris Madden. "Jitter modeling in statistical link simulation." *Electromagnetic Compatibility, 2008. EMC 2008. IEEE International Symposium on*. IEEE, 2008.

[6]   Oh, Kyung Suk Dan, and Xing Chao Chuck Yuan. *High-Speed Signaling: Jitter Modeling, Analysis, and Budgeting*. Prentice Hall, 2011.

[7]   Li, Mike Peng. *Jitter, noise, and signal integrity at high-speed*. Pearson Education, 2007.

[8]   Oppenheim, Alan V., Ronald W. Schafer, and John R. Buck. "Discrete-time signal processing." Vol. 2. Englewood Cliffs: Prentice-hall, 1989.

[9]   Shaarawi, Amr M., and Sedki M. Riad. "Computing the complete FFT of a step-like waveform." *Instrumentation and Measurement, IEEE Transactions on* 1001.1 (1986): 91-92.

[10]   Paul, Clayton R. "Introduction to electromagnetic compatibility". Vol. 184. John Wiley & Sons, 2006.

VITA

Xinyun was born in Xianyang, Shaanxi, China. She received her B.S. and M.S. degrees in Electrical Engineering from Missouri University of Science and Technology University in 2009 and 2016, respectively. She worked and studied at EMC laboratory as a research assistant, working on crosstalk analysis between high speed differential links. Her research interests include signal and power integrity for high speed digital designs.